energies

MDPI

Article

Master–Slave Game Optimization Scheduling of Multi-Microgrid Integrated Energy System Considering Comprehensive Demand Response and Wind and Storage Combination

Hongbin Sun *, Hongyu Zou *, Jianfeng Jia, Qiuzhen Shen, Zhenyu Duan and Xi Tang

School of Electrical Engineering, Changchun Institute of Technology, Changchun 130012, China
* Correspondence: dq_shb@ccit.edu.cn (H.S.); zouhongyu@stu.ccit.edu.cn (H.Z.)

Abstract: This paper addresses the critical challenge of scheduling optimization in regional integrated energy systems, characterized by the coupling of multiple physical energy streams (electricity, heat, and cooling) and the participation of various stakeholders. To tackle this, a novel multi-load and multi-type integrated demand response model is proposed, which fully accounts for the heterogeneous characteristics of energy demands in different campus environments. A leader–follower two-layer game equilibrium model is introduced, where the system operator acts as the leader, and campus load aggregators, energy storage plants, and wind farm operators serve as followers. The layer employs an enhanced particle swarm optimization (PSO) algorithm to iteratively adjust energy sales prices and response compensation unit prices, influencing the user response plan through the demand response model. In the lower layer, the charging and discharging schedules of energy storage plants, wind farm energy supply, and outputs of energy conversion devices are optimized to guide system operation. The novelty of this approach lies in the integration of a game-theoretic framework with advanced optimization techniques to balance the interests of all participants and enhance system coordination. A case study is conducted to evaluate the effectiveness of the proposed strategy, demonstrating significant economic benefits. The results show that the model encourages stakeholders to invest in energy infrastructure and actively participate in coordinated dispatch, leading to improved overall system efficiency and comprehensive revenue enhancement for the multi-agent energy system.

Keywords: multi-entity integrated energy system; two-tier optimization; improved particle swarm; integrated demand response; master-slave game

Citation: Sun, H.; Zou, H.; Jia, J.; Shen, Q.; Duan, Z.; Tang, X. Master–Slave Game Optimization Scheduling of Multi-Microgrid Integrated Energy System Considering Comprehensive Demand Response and Wind and Storage Combination. *Energies* **2024**, *17*, 5762. https://doi.org/10.3390/en17225762

Academic Editors: Anna Pinnarelli and Tek Tjing Lie

Received: 10 September 2024
Revised: 24 October 2024
Accepted: 15 November 2024
Published: 18 November 2024

1. Introduction

Amidst the escalating global greenhouse effect and energy crisis, the conflict between human society's energy demands and the natural environment's carrying capacity has become increasingly acute [1]. The integrated energy system (IES), which facilitates the coupling of multiple heterogeneous energy subsystems—such as electricity, natural gas, heating, and transportation—has emerged as a significant research focus [2,3]. As the foundational coupling terminal of the multi-energy system, the park IES holds substantial practical significance in locally consuming renewable energy, enhancing the flexibility of demand-side dispatching, and achieving the synergistic utilization of multi-energy complements [4].

The future park IES will integrate distributed clean power generation; combined heat and power (CHP) units; combined heat, power, and cooling (CCHP) units; electric vehicles (EVs); energy storage stations (EESs); flexible loads; and other units with varied attributes. Market behavior will become more flexible and complex, leading to intensified market competition [5,6]. "With the continued development of integrated energy systems,

it is anticipated that multiple systems will coexist within a single regional distribution network, thereby forming an integrated energy system cluster [7]. Zhou Xiaoxin, an academician of the Chinese Academy of Sciences, projected during the "2018 National Energy Internet Conference" that China's installed wind power capacity is expected to increase to 26.7% by the year 2050 [8]. As China's installed wind power proportion increases and the costs of distributed wind power generation remain high, large-scale wind farms, as independent entities participating in scheduling, will become a focal point of future research. In the context of future large-scale grid integration of new energy, the power system must address the challenge of mismatching new energy output with load demand [9]. Research [10] examined the impact of cluster effects on power across different wind farm cluster layouts, revealing that staggered distribution of wind farms within a cluster can enhance overall power output. However, the inconsistency and intermittency of renewable energy sources pose operational risks to the power system, such as frequency and voltage stability issues [11].

An energy storage system (ESS) utilized in a power grid is typically independently controlled and operates in three states: charging, storing, and discharging. It retains the energy generated within the power grid and releases the stored energy back to the grid when required [12]. The deployment of energy storage systems (ESSs) is widely acknowledged as a feasible solution to mitigate the operational risks associated with renewable energy sources. Energy storage is also crucial for energy management, frequency regulation, peak shaving, load balancing, seasonal storage, and backup power generation during faults, thereby facilitating the integration of renewable energy sources with the grid [13]. Existing research on energy storage power plants predominantly focuses on their service models [14,15] or considers them as independent entities to analyze their economics [16], often neglecting the interactions of inter-subjective interests. Consequently, constructing energy storage power stations and centralized wind farms within the system, and integrating them as active participants in scheduling, will establish a multi-agent integrated energy system (MIES) [17]. When power interactions occur between entities, coupled with the autonomous response behavior of users, complex benefit interactions emerge, posing significant challenges to centralized optimal scheduling. Therefore, achieving optimal scheduling within MIES, which accounts for the game-like interactions between entities, is of paramount importance [18]. Significant research progress has been made in MIESs (multiple integrated energy systems) and multi-microgrid systems [19–28]. In [19], a precise model for interconnected energy hubs is established, and an integrated strategy combining a linear weighted sum and the grasshopper optimization algorithm is proposed to address energy management, improve overall energy efficiency, and achieve regional coordinated optimization. However, this model does not account for the interaction of interests between microgrids. In [20], a comparative study on power trading among multiple microgrids, composed of heterogeneous building communities with electric vehicles (EVs), is conducted. The study employs a peer-to-peer (P2P) power trading paradigm based on hybrid game theory and compares it with the traditional time-of-use (TOU) strategy under a peer-to-grid (P2G) model. In [21], effective multi-microgrid operation strategies are developed to balance stakeholder interests, exploring collaborative operation mechanisms and strategies under different trading modes, while offering insights into future research directions. In [22], a cooperative game model for multiple microgrids is constructed to determine the interaction power with the distribution network and the charging/discharging arrangements for energy storage modules. The study employs Nash bargaining to coordinate the distribution of interests among microgrids, analyzes optimal trading power and electricity prices, and demonstrates that cooperative games can enable flexible consumption of regional renewable energy. In [23], an active control strategy for multi-microgrids under fault scenarios is proposed. In [24], a hierarchical optimization scheme for multi-microgrids is introduced, integrating energy management, optimized operation, and coordinated control. In [25], the black start process and load recovery sequence are studied based on hierarchical control in multi-microgrid systems. In [26], an optimal scheduling model for uncertain multi-

microgrid operation is developed, considering reliability and economic factors. In [27], an optimization strategy for cooperative multi-microgrid operation is proposed, addressing electricity price uncertainty and gaming fraud. Additionally, Ref. [28] presents a two-level optimal scheduling strategy that incorporates demand response and shared energy storage for multi-microgrids.

Ref. [20] proposes a multi-microgrid operation method based on energy storage station (ESS) services for a combined cooling, heating, and power (CCHP) multi-microgrid system, where the ESS manages the coordinated operation of the energy storage and CCHP systems by charging electricity. In Ref. [21], an overall framework is presented to achieve optimal operation of a microgrid (MG) based on combined cooling, heating, and power generation (CCHP). All the aforementioned studies focus on supply-side optimization while neglecting the autonomous response behaviors of the energy-using side and the impact of interest interactions among the subjects on the MIES.

Integrated demand response (IDR) is incorporated into MIESs, playing a dual economic role: (1) IDR autonomously regulates the energy system, facilitating the operation and transfer of energy between different systems; (2) IDR optimizes user energy consumption by monitoring market energy prices and responding accordingly, thus reducing energy costs [29]. Most existing studies focus on a single type of demand response behavior [30] or multiple types of demand response behavior within a single integrated energy system [24]. In multi-subject systems, Ref. [31] establishes a demand response model based on real-time prices but does not fully account for the diverse characteristics of each subject through comprehensive refinement. In the study of incentive-based demand response, unit power transfer or response subsidy reductions use fixed time-of-use prices, significantly constraining the demand side's enthusiasm to participate in flexible grid interactions [32]. Building on the aforementioned studies, multi-type, multi-load IDR is examined within MIESs, considering the unique characteristics of each park. Real-time price comparisons are conducted via iterative optimization of response subsidy unit prices, thereby enhancing the demand side's enthusiasm for participating in flexible grid interactions.

The optimal scheduling of MIESs necessitates balancing multiple interests, and the application of game theory to address these challenges has proven highly effective, finding widespread use in the optimal scheduling of integrated energy systems. For energy interconnection systems encompassing multiple communities, Ref. [33] proposes a coordinated operation method based on a master–slave game for a distributed integrated energy system with hierarchical zoning. This method considers the interests of both the master and slave entities, thereby achieving economic, flexible, and efficient operation of MIESs. Ref. [34] proposed a master–slave game optimized scheduling strategy for MAIESs based on integrated demand response, but it did not consider the existence of alliances between parks, the complementary support role of energy storage power plants for each park, or the impact on the game interaction mechanism. Ref. [35] developed a multi-objective master–slave game optimization model, employing the alternating direction multiplier algorithm to iteratively determine the non-cooperative revenues. This model aims to maximize the revenues of shared energy storage operators and minimize the operating costs of multiple microgrids within the same solution layer, reducing precision and simultaneously weakening the influence of each entity within the system. Ref. [36] proposes a multi-integrated energy microgrid low-carbon economic operation strategy based on a two-layer Stackelberg game model, but the equilibrium solution method lacks innovation.

Building on the aforementioned research and analysis, this paper proposes a master–slave game-based two-layer optimal scheduling strategy for MAIESs incorporating integrated demand response and a wind-storage combination for MIESs with storage and wind farms. The main contributions of this paper are as follows, addressing gaps and issues identified in existing studies:

(1) While many studies have considered various types of energy trading problems, they are typically limited to a single MEMG. This paper investigates the multilevel, multi-energy trading problem within a complex MIES cluster, incorporating the participation of renewable energy sources.
(2) Addressing the insufficient consideration of multi-load and multi-type demand response behaviors in MIESs, this paper establishes a multi-level and multi-type IDR model encompassing price-based, incentive-based, and fuzzy comfort-based methods. Additionally, to address the insufficient consideration of load characteristics, different IDR methods are adopted for various types of user parks, aiming to maximize demand-side participation in flexible interactions with the power grid. To tackle the issue of fixed incentive response subsidy unit prices, this paper iteratively optimizes these prices through dynamic two-way interactions between supply and demand using improved particle swarm algorithms, thereby achieving timely adjustments in energy trading prices.
(3) Addressing the gap in existing research regarding the involvement of energy storage power stations and wind farms as active subjects in scheduling, and the lack of consideration for alliance relationships and gaming behaviors between subjects, this paper proposes a master–multiple-slave two-layer game model. This model aims to maximize the comprehensive profit of the system, with the system operator as the leader and the operators of load aggregators, storage power stations, and wind farms of various parks as followers. This approach aims to enhance the enthusiasm of interconnected entities to invest in construction and participate in unified dispatch, ultimately achieving optimal economic performance of the system through the interaction of multiple entities, including energy storage power stations and wind farms.

2. Structure of a Multi-Major Integrated Energy System

Park 1 considered in this paper is a PV park representing residential users in suburban towns. The electrical loads in Park 1 primarily serve residential users and electric vehicle charging stations, with power demands lower than the PV and wind power outputs, classifying it as a residual zero-carbon park [37]. The electrical energy demand in this park is mostly met by clean energy sources, and the willingness of users to participate in demand response is relatively low. Park 1 primarily supplies power to the power-deficient Parks 2 and 3; hence, demand response is not considered in Park 1. Park 2 is a combined heating and power (CHP) park representing industrial users, while Park 3 is a combined cooling, heating, and power (CCHP) park representing urban residents. Both parks have load demands exceeding the outputs of their photovoltaic and wind power, classifying them as power-deficient parks [38]. Due to the inclusion of energy storage in the park's power supply, and considering limitations imposed by power quality and grid connection policies, this paper does not consider reverse power transmission from the energy storage power station to the grid.

There are two-way power interactions between the distribution grid and each park, wind farms and the distribution grid, storage power plants and each park, and between the parks themselves. The power flow interactions of heterogeneous energy systems established in this paper are depicted in Figure 1. The meanings of each abbreviation are listed in Table A1 in Appendix A.

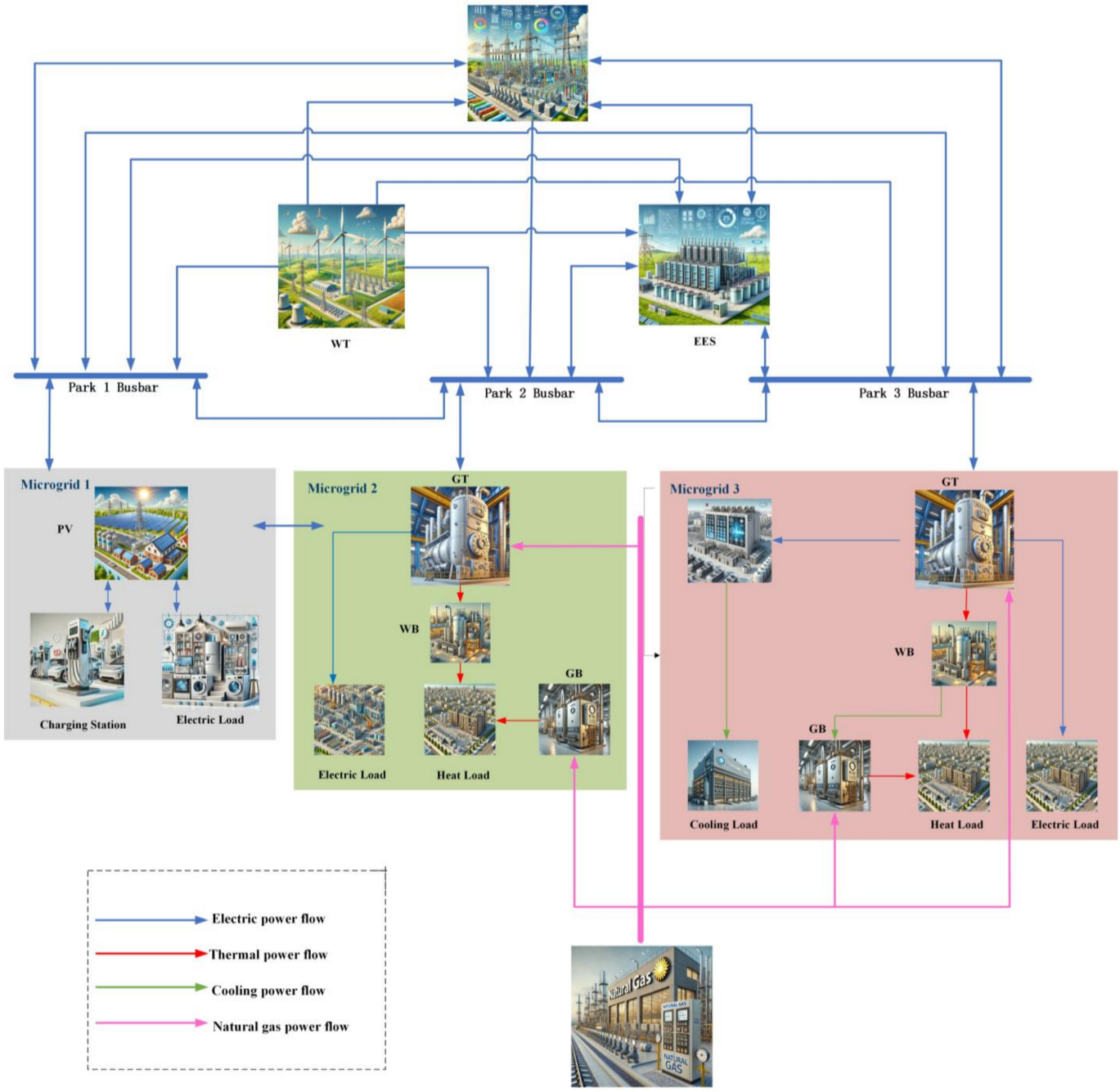

Figure 1. Operation structure of the MIES.

3. Master–Slave Game Optimization Scheduling Model for an Integrated Energy System Considering Integrated Demand Response and Multi-Entity Interaction

3.1. Integrated Demand Response Model

3.1.1. Price-Based Electric Load Demand Response Model

The electricity load response modeling in this paper adopts a price-based demand response approach. The user's electricity consumption response to price modeling involves approximately four methods, with the electricity price elasticity matrix method being the most widely used and relatively effective. Considering urban residential users are more sensitive to changes in electricity prices, this paper focuses on the price-based demand

response of electric loads [39]. According to economic principles, the elasticity coefficient of electric load is expressed as follows:

$$\varepsilon_E = \frac{\Delta p_E}{p_E} \frac{q_E}{\Delta q_E} \tag{1}$$

where Δp_E and Δq_E are denoted as the relative increments in electricity quantity p_E and electricity price q_E, respectively.

The demand-side electricity price elasticity matrix E is:

$$E_e = \begin{bmatrix} \varepsilon_{11} & \varepsilon_{12} & \cdots & \varepsilon_{14} \\ \varepsilon_{21} & \varepsilon_{22} & \cdots & \varepsilon_{24} \\ \vdots & \vdots & \ddots & \vdots \\ \varepsilon_{t1} & \varepsilon_{t2} & \cdots & \varepsilon_{tt} \end{bmatrix} \tag{2}$$

Find the power $P_{t,p}^{\text{Load,DR}}$ after the response as

$$P_{t,p}^{\text{Load,DR}} = P_t \times \Delta P_t^t = \begin{bmatrix} P_1 \\ P_2 \\ \vdots \\ P_t \end{bmatrix} + \begin{bmatrix} P_1^t & & & \\ & P_2^t & & \\ & & \ddots & \\ & & & P_t^t \end{bmatrix} E \begin{bmatrix} \frac{\Delta\sigma_1}{\sigma_1} \\ \frac{\Delta\sigma_2}{\sigma_2} \\ \vdots \\ \frac{\Delta\sigma_t}{\sigma_t} \end{bmatrix} \tag{3}$$

where P_t is the amount of electricity in the t-time period before optimization; ΔP_t^t is the amount of change in the amount of electricity in the t-time period obtained by adjusting the electricity consumption status of controllable loads after the price-based demand response of the user; ε_{tt} is the elasticity coefficient, which is taken as -0.21; and $\sigma_t, \Delta\sigma_t$ are electricity price and electricity price change, respectively.

3.1.2. Incentivized Load Demand Response Model

In Park 2, industrial users are more responsive to direct economic incentives; thus, an incentive-based load demand response is considered. The loads are classified into basic loads, transferable loads, and curtailable loads, with users being compensated based on the transfer and curtailment of their loads.

$$P_{t,q}^{\text{Load,DR}} = P_t^{\text{Base}} + P_t^{\text{Shift}} - P_t^{\text{Cut}} \tag{4}$$

$$\sum_{t=1}^{T} P_t^{\text{Shift}} = P_{\text{sum}}^{\text{Shift}} \tag{5}$$

$$\begin{cases} 0 \le P_t^{\text{Shift}} \le P^{\text{Max,Shift}} \\ 0 \le P_t^{\text{Cut}} \le P^{\text{Max,Cut}} \end{cases} \tag{6}$$

$$C_q^{\text{price,DR}} = \sum_{t=1}^{T} (P_t^{\text{Shift}} c_t^{\text{price,Shift}} + P_t^{\text{Cut}} c_t^{\text{price,Cut}}) \tag{7}$$

where P_t^{Base}, P_t^{Cut}, and P_t^{Shift} indicate the basic load, the load that can be cut, and the load that can be shifted at time t, respectively; $P_{\text{sum}}^{\text{Shift}}$ indicates the sum of the load that can be shifted in the total dispatch time t, which is a fixed value; $P^{\text{Max,Shift}}$ and $P^{\text{Max,Cut}}$ indicate the upper limit value of the load that can be cut and the load that can be cut, respectively; and $c_t^{\text{price,Shift}}$ and $c_t^{\text{price,Cut}}$ are the unit price of the unit electric power shifted and cut for compensation at time t, respectively.

3.1.3. Incentive-Type Heat Load Demand Response Model

In this paper, the heat source for heat loads 2 and 3 in the park originates from the centralized heat production of gas turbines and gas boilers, making it challenging for the load side to independently regulate the temperature. However, it is feasible to transfer and curtail the heat loads in real time; therefore, an incentive-based heat load demand response is adopted. The heat load is classified into basic heat load, transferable heat load, and curtailable heat load, with users receiving economic compensation based on the amount of load transfer and curtailment. The transferable heat load is modeled as follows:

$$\begin{cases} H_{t,start+n} = U^{\mathrm{H}}_{t,start+n} H^{\mathrm{Shift}}_{t} \\ \sum\limits_{t=1}^{T} U^{\mathrm{H}}_{t} = \sum\limits_{t=t,start}^{t,end} U^{\mathrm{H}}_{t} = t_{\mathrm{last}} \\ U^{\mathrm{H}}_{t} - U^{\mathrm{H}}_{t-1} \le B^{\mathrm{H}}_{t} \end{cases} \tag{8}$$

where H^{Shift}_{t} is the load quantity of the transferable load at time t; $t,start$, t,end is the translational range of the transferable thermal load; t_{last} is the load duration; and U^{H}_{t} and B^{H}_{t} are the operating state and start/stop state of the load at time t.

$$\begin{cases} \sum\limits_{t=t,on}^{t=t,off} H^{\mathrm{Cut}}_{t} = H^{\mathrm{Cut}}_{\mathrm{Sum}} \\ H^{\mathrm{Cut}}_{Min} \le H^{\mathrm{Cut}}_{t} \le H^{\mathrm{Cut}}_{Max} \end{cases} \tag{9}$$

$$H^{\mathrm{Load,DR}}_{t} = H^{\mathrm{Base}}_{t} + H^{\mathrm{Shift}}_{t} - H^{\mathrm{Cut}}_{t} \tag{10}$$

$$C^{H,\mathrm{DR}} = \sum_{t=1}^{T} (H^{\mathrm{Shift}}_{t} c^{\mathrm{H,Shift}}_{t} + H^{\mathrm{Cut}}_{t} c^{\mathrm{H,Cut}}_{t}) \tag{11}$$

where H^{Base}_{t} and $H^{\mathrm{Load,DR}}_{t}$ denote the basic thermal load at time t and the power of the thermal load after response; $c^{\mathrm{H,Shift}}_{t}$ and $c^{\mathrm{H,Cut}}_{t}$ are the unit price of compensation for thermal load shifting and reduction, respectively; and $c^{\mathrm{H,Cut}}_{t}$ is the compensation gain for thermal response.

3.1.4. Cold Load Demand Response Model

In this paper, the cold load in Park 3 primarily consists of air-conditioning refrigeration. Given that the load side can easily adjust the temperature, the cold load is considered a flexible, adjustable load, participating in fuzzy comfort-based cold demand response. The predicted mean vote (PMV) index is used to characterize the user's perception of the ambient temperature [40], and its expression is as follows:

$$\begin{aligned} f_{\mathrm{PMV}} = {} & (0.303\mathrm{e}^{-0.036M} + 0.0275)[M(1-\eta) - \\ & 3.054(5.765 - 0.007H - P_a) - 0.42(H - 58.15) \\ & -0.0173M(5.867 - P_a) - 0.0014M(34 - T_a) - \\ & 3.9 \times 10^{-8} f_{cl}(T^4_{cl} - T^4_{mrt}) - f_{cl} h_{cl}(t_{cl} - T_a)] \end{aligned} \tag{12}$$

where M is the metabolic rate, e represents a constant; η is the rate of heat dissipation from the body; t_{cl} is the average surface temperature of the body; T_{mrt} is the average ambient radiant temperature; H represents the absolute humidity of air, usually expressed in g/kg; P_a indicates the water vapor pressure of air; T_a indicates air temperature; f_{cl} indicates the coefficient related to the thermal resistance of clothing; and h_{cl} A represents the coefficient related to convective heat transfer.

$$\begin{cases} C^{\mathrm{Load,DR}}_{t,cold} = S\mu(T_{\mathrm{out},t} - T_{\mathrm{in},t}) + (CS/\Delta t)(T_{\mathrm{in},t} - T_{\mathrm{in},t-1}) \\ T_{\min} \le T_{\mathrm{in},t} \le T_{\max} \end{cases} \tag{13}$$

where $C_{t,cold}^{\text{Load,DR}}$ is the power of cold load; S is the cooling area; μ is the heat loss under the unit temperature difference of the unit cooling area, and is taken as 1.037×10^4 J/(m$^2 \cdot$ °C); C is the heat capacity of the unit cooling area, which is taken as 1.63×10^5 J/(m$^2 \cdot$ °C); and $T_{\text{in},t}$ and $T_{\text{out},t}$ are the indoor/outdoor temperature at time t.

3.2. Charging and Discharging Strategy and Revenue Model of Energy Storage Plant

The existing issues of high investment costs, prolonged cost recovery cycles, and low safety and reliability of user-side distributed energy storage systems limit their widespread adoption [41]. To address these challenges, this paper proposes the establishment of a systematic centralized energy storage power station that:

$$\begin{aligned} C^{EES} = \sum_{t=1}^{T} \{ \sum_{j=1}^{N} [(c_t^{EES} + \varphi) P_{j,t}^{\text{Ch}}] - \\ \sum_{j=1}^{N} [(c_t^{\text{p,sell}} + \psi) P_{j,t}^{\text{Dis}}] + (c_t^{EES} + \varphi) P_t^{\text{Ch,Grid}} + (c_t^{EES} + \varphi) P_t^{\text{Ch,Wind}} \} \end{aligned} \tag{14}$$

$$c_t^{EES} = c_t^{EES,\text{sell}} + \tau \tag{15}$$

where $P_{j,t}^{\text{Ch}}$, $P_{j,t}^{\text{Dis}}$, $P_t^{\text{Ch,Grid}}$, and $P_t^{\text{Ch,Wind}}$ denote the power of the storage plant to discharge to the park, charge, charge from the superior grid, and charge from the centralized wind farm, respectively; τ denotes the unit revenue of the storage plant participating in the auxiliary services; $c_t^{EES,\text{sell}}$ and c_t^{EES} are the basic selling price and comprehensive selling price of the storage plant, respectively; and φ and C^{EES} are the operation and maintenance cost and profit of the storage plant per unit of power, respectively.

3.3. Energy Supply Strategy and Revenue Model for Centralized Wind Farms

In this paper, we propose to establish a systematic centralized wind farm, which is coordinated and controlled by a MAIES and participates in centralized dispatching.

$$C^{\text{Wind}} = \sum_{t=1}^{T} [(P_t^{\text{Ch,Wind}} + P_t^{\text{Wind,Grid}} + \sum_{j=1}^{N} P_{j,t}^{\text{Wind}}) \cdot (c_t^{\text{Wind,sell}} - c^{\text{Wind},P})] \tag{16}$$

In the formula, $P_t^{\text{Wind,Grid}}$ and $P_{j,t}^{\text{Wind}}$ represent the power sold by the wind farm to the distribution grid and the park at time t, respectively. $c_t^{\text{Wind,sell}}$, $c^{\text{Wind},P}$, and C^{Wind} represent the wind farm's electricity sale price, the operational E, and the profit per unit of power, respectively.

3.4. Objective Function

$$F_{\max} = \sum_{j=1}^{N} C_j + C^{\text{EES}} + C^{\text{Wind}} - C^{\text{Grid}} \tag{17}$$

$$\begin{aligned} C_j = \sum_{t=1}^{T} (E_{j,t}^{\text{Load,DR}} c_t^{E,\text{sell}} - P_{j,t}^{\text{Grid,buy}} c_t^{\text{Grid,sell}} - G_{j,t}^{Gas} c_t^{\text{Gas}} - P_{j,t}^{\text{Dis}} c_t^{ESS,\text{Dis}} \\ + P_{j,t}^{\text{Ch}} c_t^{ESS,\text{ch}} - P_{j,t}^{\text{Wind}} c_t^{\text{Wind,sell}} - P_{j,t}^{\text{B}} c_t^{\text{B,p}}) \end{aligned} \tag{18}$$

$$\begin{aligned} C^{\text{Grid}} = \sum_{t=1}^{T} [\sum_{j=1}^{N} (P_{j,t}^{\text{Grid,buy}} c_t^{\text{Grid,sell}} - P_{j,t}^{\text{Grid,sell}} c_t^{\text{Ex,sell}} - C_j^{E,\text{DR}}) \\ + P_t^{\text{Ch,grid}} c_t^{\text{Ess,Grid}} - P_t^{\text{Wind,Grid}} c_t^{\text{Wind,sell}}] \end{aligned} \tag{19}$$

where F is the total profit of the MIES; N denotes the number of parks, which is 3 in this paper; T denotes the total dispatch time, which is 24 h in this paper; C_j is the economic compensation paid by the distribution network to the demand response behavior of the users in the park j; $E_{j,t}^{\text{Load,DR}}$ is the user's demand response to energy source E; E is the set of

electricity, heat, and cooling load types; $c_t^{E,\text{sell}}$ is the unit price of energy sold to the users in the park at time t; $c_t^{\text{B,p}}$ is the operation and maintenance cost per unit power of equipment B in the park j, including the operation and start/stop costs; $c_t^{\text{Grid,sell}}$ and $c_t^{\text{Ex,sell}}$ are the unit price of electricity sold by the distribution network and the park, respectively; c_t^{Gas} is the price of natural gas; the prices of which can be found in Table A2 in Appendix A; $G_{j,t}^{\text{Gas}}$ is the purchased gas power of the park at time t; and C^{Grid} is the profit of the distribution network.

3.5. Constraints

Electrical Power Balance Constraints

$$P_{j,t}^{\text{Grid,buy}} + P_{j,i,t}^{\text{buy}} - P_{j,i,t}^{\text{sell}} + P_{j,t}^{\text{Dis}} - P_{j,t}^{\text{Ch}} + P_{j,t}^{\text{Wind}} + P_{j,t}^{PV} + P_{j,t}^{CHP} - P_{j,t}^{\text{Air}} = P_{j,t}^{\text{Load,DR}} \tag{20}$$

where $P_{j,t}^{\text{Grid,buy}}$, $P_{j,t}^{PV}$, and $P_{j,t}^{\text{Air}}$ denote the power purchased from the distribution grid, distributed photovoltaic power generation, and air-conditioning power consumption of the park at time t, respectively. Since the CCHP unit in the system is converted from the CHP unit by adding a lithium bromide refrigerator, $P_{j,t}^{CHP}$ is expressed as a unified expression, which represents the power generated by the CHP unit at the moment of t in Park 2 and the power generated by the CCHP unit at the moment of t in Park 3. $P_{j,i,t}^{\text{buy}}$ and $P_{j,i,t}^{\text{sell}}$ represent the power purchased and sold from Park j to Park i.

(1) Thermal power balance constraint.

$$Q_{j,t}^{\text{Chp}} + Q_{j,t}^{\text{Bo}} = Q_{j,t}^{\text{Load,DR}} \tag{21}$$

where $Q_{j,t}^{\text{Chp}}$ and $Q_{j,t}^{\text{Bo}}$ denote the heat production power of the CHP unit and the gas boiler in the park j at time t, respectively.

(2) Cold power balance constraints.

$$C_{j,t}^{CCHP} + C_{j,t}^{\text{Air}} = C_{j,t}^{\text{Load,DR}} \tag{22}$$

where $C_{j,t}^{CCHP}$ and $C_{j,t}^{\text{Air}}$ denote the cooling power of the CCHP unit and the air conditioner in the park j at time t, respectively.

(3) Inter-park power transfer constraints.

$$\sum_{j=1}^{N}\sum_{t=1}^{T} P_{j,t}^{\text{buy}} = \sum_{j=1}^{N}\sum_{t=1}^{T} P_{j,t}^{\text{sell}} \tag{23}$$

$$\begin{cases} 0 \le P_{j,i,t}^{\text{buy}} \le P_{j,i}^{\text{buy,Max}} B_{j,i,t}^{\text{buy}} \\ 0 \le P_{j,i,t}^{\text{sell}} \le P_{j,i}^{\text{sell,max}} B_{j,i,t}^{\text{sell}} \\ B_{j,i,t}^{\text{buy}} + B_{j,i,t}^{\text{sell}} \le 1 \end{cases} \tag{24}$$

where $P_{j,t}^{\text{buy}}$, $P_{j,t}^{\text{sell}}$, $P_{j,i}^{\text{buy,}Max}$, $P_{j,i}^{\text{sell,max}}$, $B_{j,i,t}^{\text{buy}}$, and $B_{j,i,t}^{\text{sell}}$ denote the purchased and sold power, the upper limit of purchased and sold power, and the 0–1 variable of purchased and sold power behavior from the park j to the park at moment i.

(4) Park and distribution grid power transfer constraints.

$$\begin{cases} 0 \le P_{j,i,t}^{\text{buy}} \le P_{j,i}^{\text{buy,Max}} B_{j,i,t}^{\text{buy}} \\ 0 \le P_{j,i,t}^{\text{sell}} \le P_{j,i}^{\text{sell,Max}} B_{j,i,t}^{\text{sell}} \\ B_{j,i,t}^{\text{buy}} + B_{j,i,t}^{\text{sell}} \le 1 \end{cases} \tag{25}$$

where $P_{j,i}^{\text{buy,Max}}$, $P_{j,i}^{\text{sell,Max}}$, $B_{j,i,t}^{\text{buy}}$, and $B_{j,i,t}^{\text{sell}}$ denote the upper limit of power purchased and sold to the distribution grid by the park j at time t and the 0–1 variable of power purchasing and selling behavior, respectively.

(5) Centralized energy storage plant operational constraints.

$$P_t^{\text{SOC}} = P_{t-1}^{\text{SOC}} + \eta^{\text{Ch}} \cdot (\sum_{j=1}^{N} P_{j,t}^{\text{Ch}} + P_t^{\text{Ch,Grid}} + P_t^{\text{Ch,Wind}}) - \eta^{\text{Dis}} \sum_{j=1}^{N} P_{j,t}^{\text{Dis}} \tag{26}$$

$$\begin{cases} P_{\text{Min}}^{\text{SOC}} \le P_t^{\text{SOC}} \le P_{\text{Max}}^{\text{SOC}} \\ P_{t=1}^{\text{SOC}} = P_{t=T}^{\text{SOC}} = P_{on}^{\text{SOC}} \\ 0 \le P_{j,t}^{\text{Ch}} \le P_{\text{ch}}^{\text{Max}} B_{j,t}^{\text{Ch}} \\ 0 \le P_{j,t}^{\text{Dis}} \le P_{\text{dis}}^{\text{Max}} B_{j,t}^{\text{Dis}} \\ 0 \le P_t^{\text{Ch,Grid}} \le P_{\text{ch}}^{\text{Max}} B_t^{\text{Ch,Grid}} \\ 0 \le P_t^{\text{Ch,Wind}} \le P_{\text{ch}}^{\text{Max}} B_t^{\text{Ch,Wind}} \\ B_{j,t}^{\text{Ch}} + B_{j,t}^{\text{Dis}} \le 1 \end{cases} \tag{27}$$

where P_t^{SOC}, $P_{\text{Min}}^{\text{SOC}}$, and $P_{\text{Max}}^{\text{SOC}}$ denote the charging state and upper- and lower-limit values of the energy storage power station; η^{Ch} and η^{Dis} denote the charging and discharging efficiency; $B_{j,t}^{\text{Ch}}$ and $B_{j,t}^{\text{Dis}}$ denote the charging and discharging behavior of the energy storage power station to the park j at time t; $B_t^{\text{Ch,Grid}}$ and $B_t^{\text{Ch,Wind}}$ are the purchasing behavior of the energy storage power station to the distribution grid and the wind farm at time t. The maximum charging and discharging power are $P_{\text{ch}}^{\text{Max}}$ and $P_{\text{dis}}^{\text{Max}}$, respectively.

(6) Centralized wind farm output constraints.

$$\sum_{j=1}^{N} P_{j,t}^{\text{Wind}} + P_t^{\text{Ch,Wind}} + P_t^{\text{Wind,Grid}} = P_t^{\text{Wind}} \tag{28}$$

$$\begin{cases} 0 \le P_t^{\text{Wind}} \le P_t^{\text{Wind,Max}} B_t^{\text{Wind}} \\ 0 \le P_t^{\text{Wind,Grid}} \le P^{\text{Wind,Grid,Max}} B_t^{\text{Wind,Grid}} \\ 0 \le P_t^{\text{Ch,Wind}} \le P^{\text{Ch,Wind,Max}} B_t^{Ch,\text{Wind}} \end{cases} \tag{29}$$

where B_t^{Wind} and $B_t^{\text{Wind,Grid}}$ are the 0–1 variables for power sales from the wind farm to the park and the distribution grid, respectively, at time t.

3.6. Master–Slave Game Interaction Mechanism

This paper presents a master–multiple-slave MIES two-layer game model, with the interaction mechanism illustrated in Figure 2. The game interaction in the MAIES is structured into two layers: an upper layer and a lower layer, with a sequential relationship and interactive iteration. The model solution process is outlined in the upper part of Figure 3. This flowchart presents a two-layer optimization framework for a multi-agent integrated energy system (MAIES), which combines particle swarm optimization (PSO) and CPLEX for energy trading and operation management. The system handles energy trading and real-time energy management within energy parks, incorporating multi-objective optimization, such as minimizing costs and maximizing profits. The upper layer employs the particle swarm optimization algorithm to determine the optimal trading strategy for the integrated energy system. Specific steps include (1) initialization: The algorithm inputs the number of particles, maximum iterations, and accuracy; (2) speed and position update: The speed and position of each particle are dynamically updated via PSO, influenced by their historical best position and the global best position; (3) energy consumption strategy update: The energy consumption and trading strategy for each energy park is updated based on the latest particle positions, which reflect the updated energy market decisions; (4) fitness calculation: The fitness function is computed for each particle, typically

combining objectives such as profit maximization, cost minimization, and system stability; (5) local and global optimal update: If the current particle's fitness exceeds its previous value, the local and global optimal solutions are updated accordingly; and (6) iteration check: If the number of iterations does not exceed the maximum or the required accuracy is not met, the iteration count increases by 1, and the process repeats until convergence.

After the upper-layer PSO algorithm converges, the lower layer uses CPLEX to optimize energy coupling and operation strategy in the MAIES. Specific steps include (1) price generation: Based on the upper layer results, the MAIES determines the energy sales price for users and the compensation price for demand response; (2) park energy user operation: Integrated energy users adjust their operation based on real-time energy prices and incentives, and the demand response system adjusts the park's actual load and calculates the energy purchase cost; (3) CPLEX optimization: The system uses CPLEX to optimize energy coupling conversion equipment, focusing on energy flow, conversion efficiency, and minimizing operational costs; (4) profit calculation: The MAIES' current profit is calculated and compared with the previous iteration to check for improvement; and (5) profit optimization check: If the current iteration's profit exceeds the previous one, the MAIES' optimal profit is updated. This process continues until the profit stabilizes. Termination condition: The optimization framework terminates once the MAIES' optimal profit stabilizes, indicating that the system has reached a steady-state solution for energy trading and operation strategy. The specific details of the algorithm are shown in Appendix B.

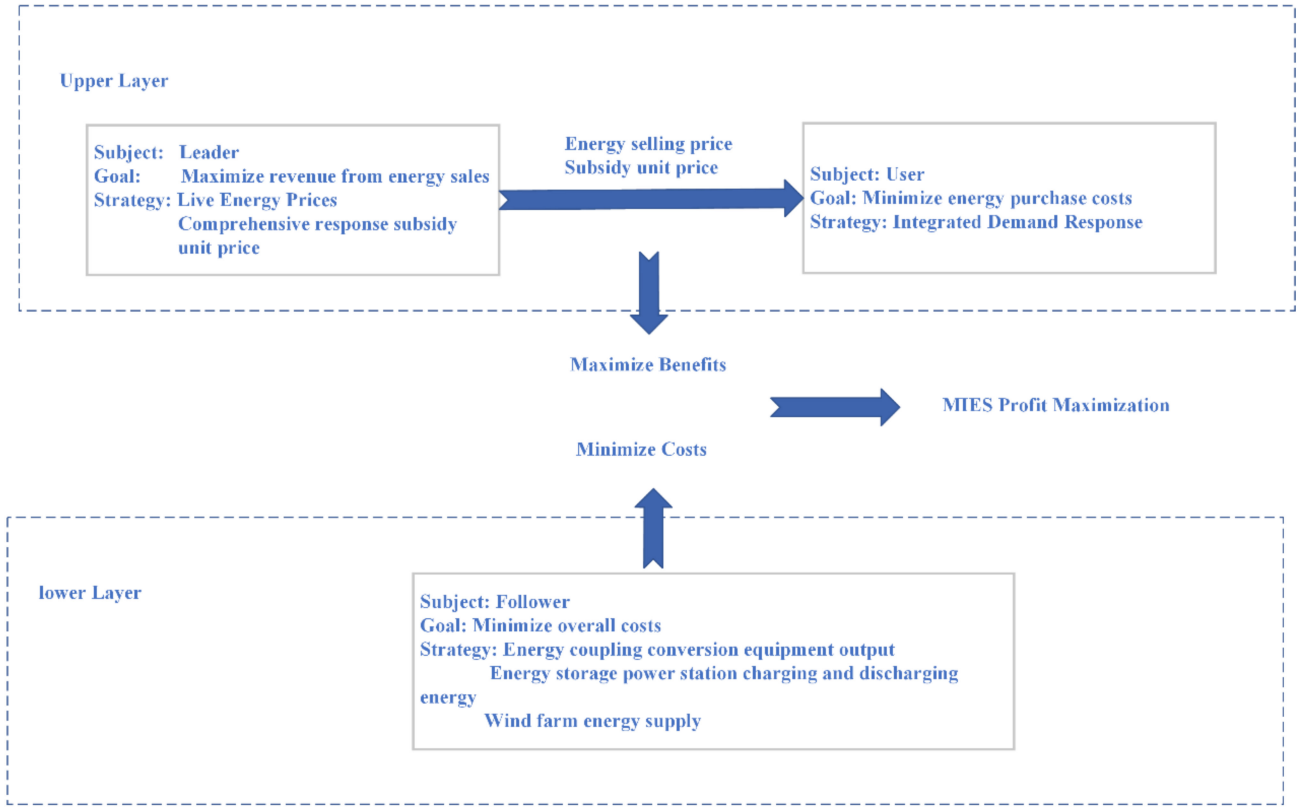

Figure 2. Master–slave game.

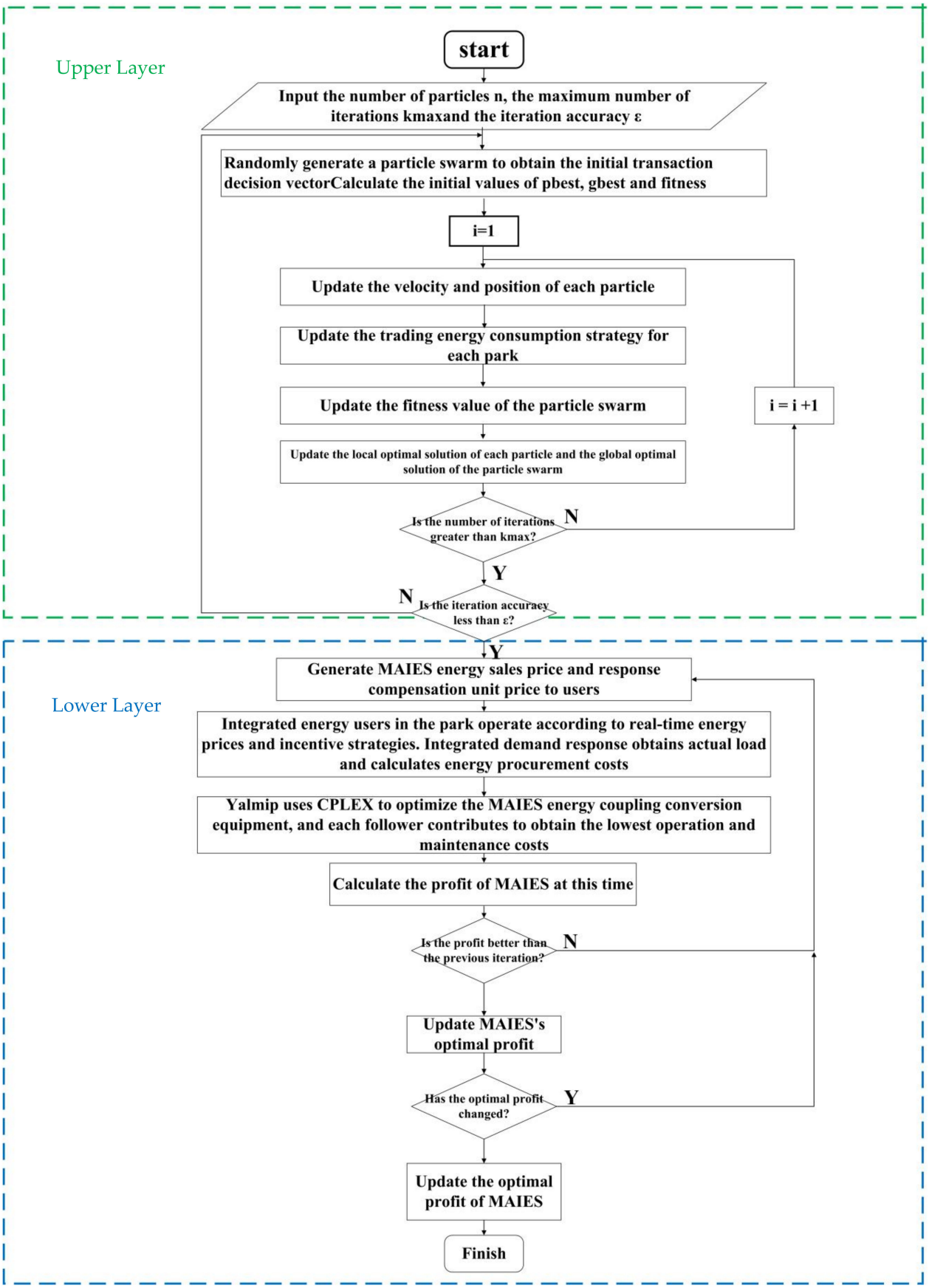

Figure 3. Model solution process.

Each park's load aggregators act as followers, aiming to minimize electricity purchasing costs. Their strategy set includes responding to power restrictions, transfers, and substitution scenarios. Energy storage power stations and centralized wind farms also act as followers, aiming to maximize their profits. Their strategies involve managing charging/discharging activities and power supply. The leader sets the electricity price and subsidy for demand response and communicates this to the follower park users. Users respond to the electricity price and subsidy, and determine their electricity purchase costs, and this forms the revenue for the MIES. The MIES revenue is determined at the upper layer, while the output of energy conversion devices, the charging/discharging of energy storage, and wind farm power supply are adjusted based on the external grid price and energy constraints. This process optimizes the MIES' costs. The total daily profit is calculated by combining both layers, and the process repeats until the optimal solution is reached, achieving balance. This suggests that the park achieves total profit in the multi-agent system by optimally allocating each entity's interests, assuming a complete information game, where the system operator (leader) can enforce constraints on entities through executable contracts. In summary, this study addresses the distribution of benefits after cooperation is achieved, formed the context of campus alliance cooperation. The proof of the Nash equilibrium solution for the game is provided in Appendix C.

4. Example Analysis

In this section, the effectiveness and rationality of the proposed master–slave game optimal scheduling for integrated energy systems, considering integrated demand response and multi-agent interaction, will be verified through algorithmic analysis.

4.1. Arithmetic Example Setup

In this paper, the IES with multiple entities, as depicted in Figure 1, is selected for simulation calculations. The MAIES consists of energy operators, customer clusters containing PV, CHP parks, CCHP parks, energy storage plants, and centralized wind power generation entities, all interconnected by transmission lines. Each park comprises integrated energy users and is managed by a load aggregator. The price at which each park purchases/sells electricity from/to other parks is a flat rate, which is lower than the price at which electricity is purchased/sold from the external distribution network. The distribution network sales price, the natural gasprice, and the price of electricity interactions within and outside the parks are shown in Table A1 in Appendix A. The system's energy conversion coupling equipment parameters are shown in Appendix A Table A2. The predicted electrical load and photovoltaic output values are provided in Appendix D.

4.2. Scenario Setting

To illustrate the reasonableness and feasibility of the proposed optimization strategy, various operation scenarios are compared:

(1) Scenario 1: To verify the validity and economy of non-interconnection among multiple entities, this setup does not consider the interaction of electricity between parks, meaning operations are independent, with no cooperative alliance.
(2) Scenario 2: To validate the effectiveness and economics of centralized wind farms, this scenario sets up a multi-campus interconnection based on Scenario 1, considering the operation of centralized wind farms.
(3) Scenario 3: To verify the effectiveness and cost-effectiveness of an energy storage plant, this scenario sets up a multi-campus interconnection based on Scenario 1, considering the operation of a centralized energy storage plant.
(4) Scenario 4: To verify the effectiveness and economics of integrated demand response and iterative optimization of subsidy unit prices, this scenario sets up an operation mode based on Scenario 3, considering integrated demand response and iterative optimization of subsidy unit prices after interaction among multiple actors.

(5) Scenario 5: This scenario implements the strategy proposed in this paper, considering the master–slave game optimization scheduling of a multi-entity integrated energy system with integrated demand response and wind storage.

After optimization calculations, the cost of purchased energy, revenue from energy sales, profit of each entity, and comprehensive profit of the MAIES for each operation mode under each scenario are determined, as shown in Table 1.

Table 1. Results of optimization calculation.

Scenario	Purchased Electricity Cost/RMB	Gas Purchase Cost/RMB	Park 1 Profit/RMB	Park 2 Profit/RMB	Park 3 Profit/RMB	Profit of Energy Storage Plant/RMB	Wind Farm Profit/RMB	Demand Response Compensation/RMB	MIES Total Profit/RMB
1	13,061	22,285.5	2567	9421	11,931	3091	—	—	38,331
2	12,170	22,285.5	1351	14,821	13,731	—	13,932	7434	39,400
3	18,853	16,527	3562	15,992	16,138	585	—	7534	34,389
4	11,863	22,285.5	1317	14,431	13,536	2331	13,920	7091	40,716
5	12,352	22,285.5	1343	14,621	13,088	2361	13,920	7429	41,441

4.3. Comparative Analysis

Scenario 1 does not incorporate any optimization methods; each park operates independently without the addition of the wind storage joint system, serving as the baseline scenario.

Scenario 2 incorporates centralized wind power, enabling the effective use of new energy and participation in the park's energy supply. This reduces the power purchased from the distribution grid, saving CNY 891 in power purchase costs. In the suburbs, Park 1 benefits from substantial PV resource endowment, producing much more new energy than the other parks while having low self-consumption. Consequently, it sells a large amount of electricity to the other parks. However, with the addition of centralized wind farms, many users opt to purchase the lower-priced electricity from the wind farms, significantly reducing Park 1′s profit while increasing the profit of the wind farm. As a result, the profit of the MIES increases by CNY 1069. This demonstrates that increasing new energy consumption can effectively improve system profits, and constructing centralized wind farms in wind-rich areas and incorporating them into MAIES scheduling can maximize the system's comprehensive profit.

Scenario 3 incorporates an energy storage power station. During periods of high new energy output and low electricity prices, energy is stored, and during peak load periods, this energy is discharged. The centralized energy storage power station has lower operation and maintenance costs. Although its standalone participation in MIES optimization scheduling is not very impactful, it significantly benefits parks with large load regulation ranges. Compared to Scenario 1, the parks' profits increase by CNY 995, CNY 5571, and CNY 4207, respectively. This demonstrates that electric energy storage enhances the economics of each park.

In Scenario 4, the total profit for the MAIES is reported as 40,716 MB, derived from the combined profits of all energy participants, including the parks, energy storage plant, wind farm, and demand response. This total profit reflects the system's optimal performance under Scenario 4, showcasing a balanced integration of diverse energy sources, optimized transaction strategies, and cost-efficient operation. The results indicate that Scenario 4 is highly profitable for the MAIES, primarily due to strong contributions from the wind farm and Park 3, along with the beneficial role of the energy storage plant. Scenario 4 in Table 1 represents an optimized configuration of the multi-agent integrated energy system (MAIES), balancing electricity and gas purchase costs with profits from energy parks, energy storage, and renewable energy sources. This scenario highlights the importance of coordinated energy management, where distributed generation, storage, and demand response play key roles in ensuring system profitability and operational efficiency. The detailed breakdown of costs and profits offers valuable insights into the economic and technical viability of

the MAIES, especially in scenarios with high renewable energy penetration and effective demand-side management.

In Scenario 5, through iterative optimization of subsidy unit prices and double-layer optimization of the multi-party game, the transfer and curtailment of peak period loads are increased, reducing power purchase costs and improving response compensation. The profit of the MIES increases by 6327 RMB, an 18.39% increase. Therefore, iterative optimization of subsidy unit prices enhances users' motivation to participate in demand response, effectively improving system profits.

In summary, the master–slave game optimization scheduling of a multi-intelligent integrated energy system, considering integrated demand response and wind storage, improves system economy. This illustrates the effectiveness and rationality of the proposed strategy.

4.4. Optimization Results of the Strategy in This Paper

For the strategy and model proposed in this paper, the global optimal solution is obtained through iterative optimization in the upper and lower layers, and the problem is solved multiple times. Figure 4 shows the finalized electricity and heat prices and response compensation unit prices issued by the MAIES to users in the upper layer. It can be observed from the figure that the electricity price, after compensation through electric load reduction and transfer, is reduced by up to CNY 0.8324 and CNY 0.7 compared with the park's selling price. Similarly, the electricity price after heat load reduction and transfer compensation is reduced by up to CNY 0.451 and CNY 0.459 compared with the park's selling price.

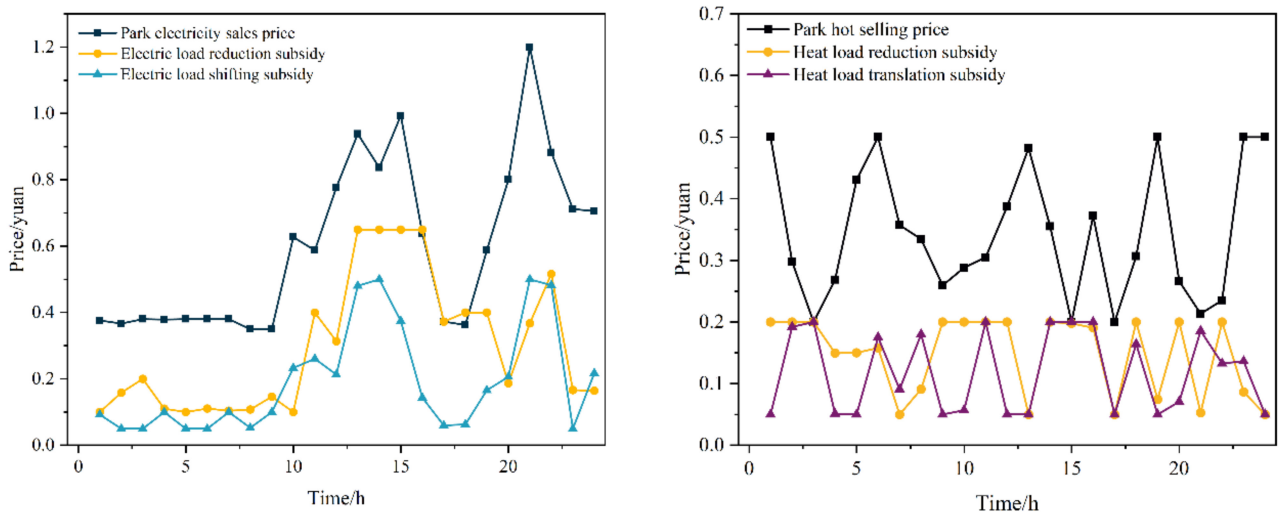

Figure 4. Optimized pricing costs for electricity and heat price incentive compensation.

From Figure 5, it can be seen that the interaction between the distribution grid and the main parks is not high, primarily concentrated at night when distribution grid tariffs are lower. Parks 1 and 2 discharge power due to a lack of supply, correlating with the load and exhibiting typical peak and valley leveling characteristics. At night, Park 1's PV clusters do not generate power, leading to a supply shortage, while Park 3's electrical load is the highest. During other periods, due to incentive compensation, the main subjects prefer trading within the MAIES, resulting in zero interaction with the distribution grid.

Figure 6 shows the comparison of electric load before and after demand response in each park. Electric load reduction and transfer are mainly concentrated in the 10:00–24:00 time period. Compared with Figure 4, during this period, the cost of optimized pricing for tariff incentives and compensation is larger than the price difference in the distribution grid. In the 00:00–10:00 time period, the tariff difference is smaller, and combined with

the cost of demand response, electric load reduction and transfer are essentially zero. The electric loads that can be cut and transferred in the three parks are 313.50 kW, 1296.39 kW, and 924.94 kW, respectively.

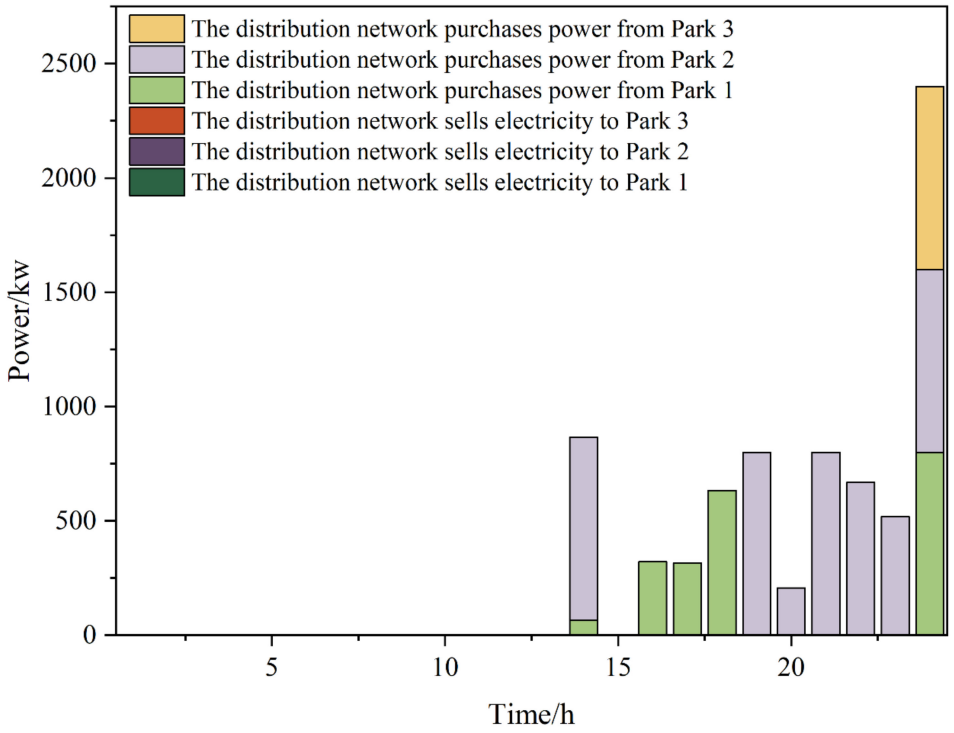

Figure 5. Interactive power values between the distribution network and the parks.

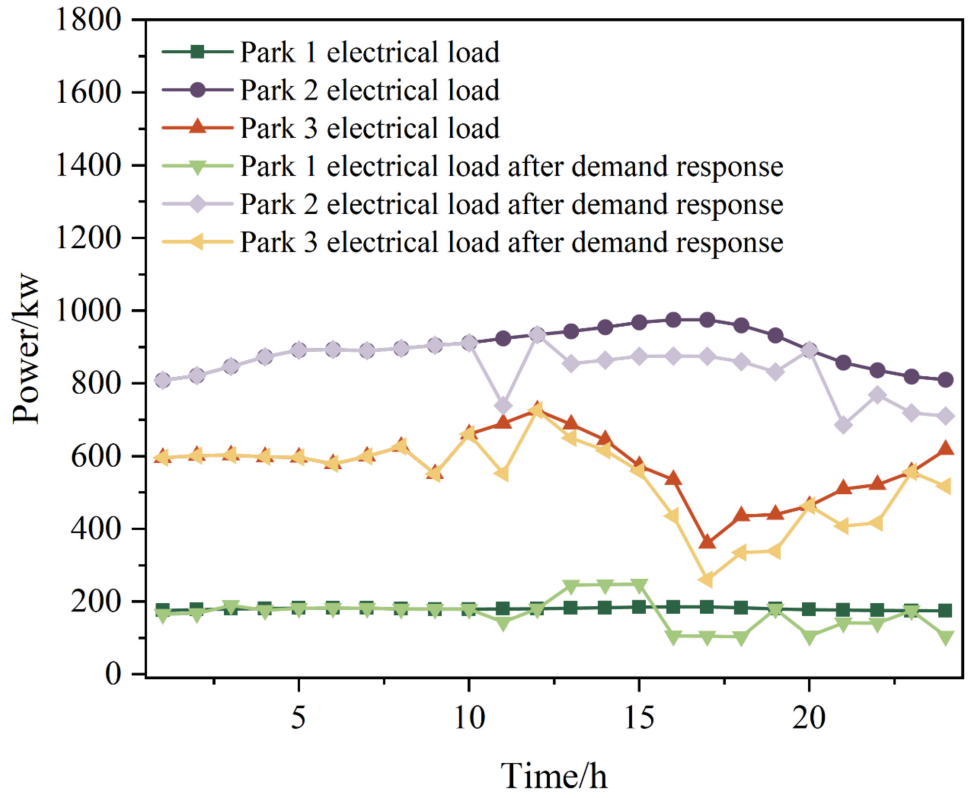

Figure 6. Before-and-after comparison of electrical load demand in each park.

Figure 7 shows the comparison of cooling and heating loads before and after demand response. There is greater demand for heating loads at night and more demand for cooling loads at midday. Due to the significant fluctuation in cooling and heating loads with temperature changes, the cooling and heating power in the "electricity to heat" mode is more noticeable and uniform compared with the electric load response.

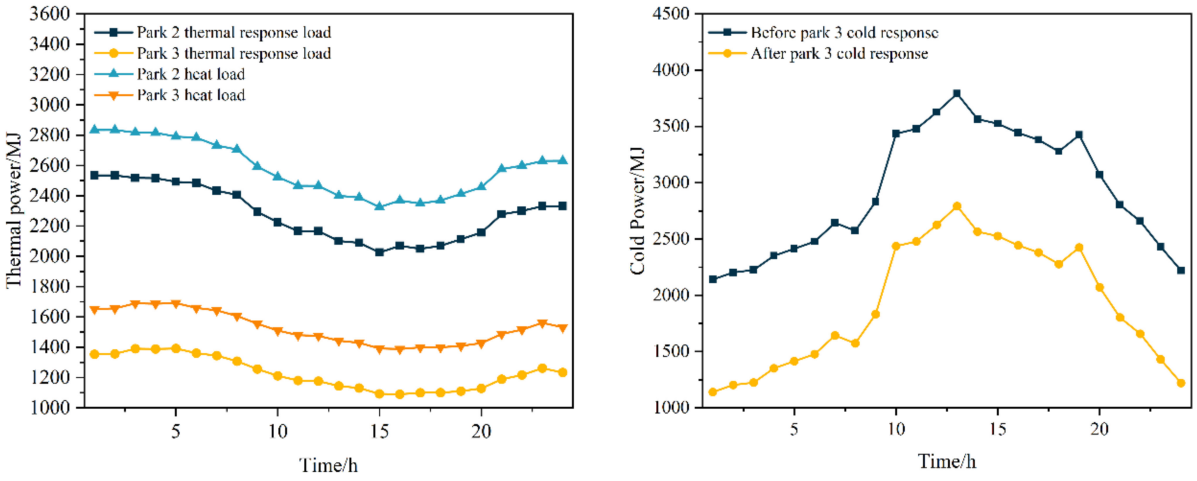

Figure 7. Before-and-after comparison of heat and cooling load demand in each park.

The power balance of the wind farm is shown in Figure 8. The state subsidizes new energy generation, so in this simulation, the unit price of the wind farm is lower than that of the distribution grid. Considering the distance from the wind farm to the park and the associated transmission losses, the time-sharing price of the wind farm falls between that of the distribution grid and the park's power interaction (see Table A2 in Appendix A for more details). As a result, the wind farm primarily operates in cooperation with the storage plant. Only when there is no photovoltaic generation in Park 1 during the morning hours and when Parks 2 and 3 experience the highest power shortages at midday does the wind farm transmit a small amount of power to them. More frequently, the centralized wind farm sells power to the distribution grid, which has a higher unit price, and to the energy storage plant, which can readily absorb uncertain wind power.

The charge/discharge power interaction value of the energy storage power station is depicted in Figure 9. Figure 9 shows that due to sufficient PV power generation from 9:00 to 17:00, the main load in Park 1 is EV charging piles, which are less loaded compared to Parks 2 and 3. Park 1, classified as a residual power park with larger power outputs, becomes the main source for power storage because the unit price of energy storage power purchased from the parks is lower than that from the distribution grid and wind farms. From 0:00 to 8:00 and from 18:00 to 24:00, when Park 1 has no power supply, the energy storage power station provides electricity to complete new energy peak shaving and valley filling.

The loads in Park 2 and Park 3 are large, and their supply is much smaller than their demand. As shown in Figure 9, the energy storage supplies power to Park 3 for 23 h a day, making Park 3 the primary outlet for energy storage discharge. The charging hours of the energy storage plant are mainly concentrated between 00:00 and 06:00 and between 17:00 and 00:00, coinciding with the electricity price trough period. The maximum capacity of the energy storage plant is reached in the early morning and evening hours, allowing the energy storage to play an effective role in supporting the energy supply during peak hours.

Figure 10 shows the optimized power balance diagram of Park 1. Since the main load in Park 1 consists of electric vehicles, classifying it as an overcapacity electric load park, a small portion of PV power is supplied to this park, while the rest is directed to the energy storage power station for effective storage of new energy generation and peak shaving and valley filling.

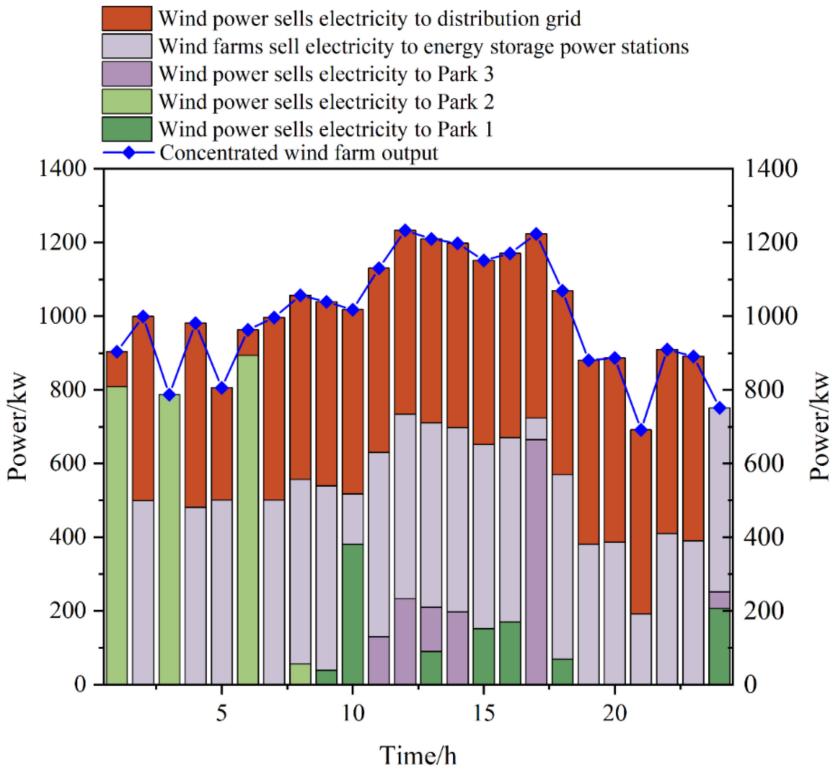

Figure 8. Wind farm power balance diagram.

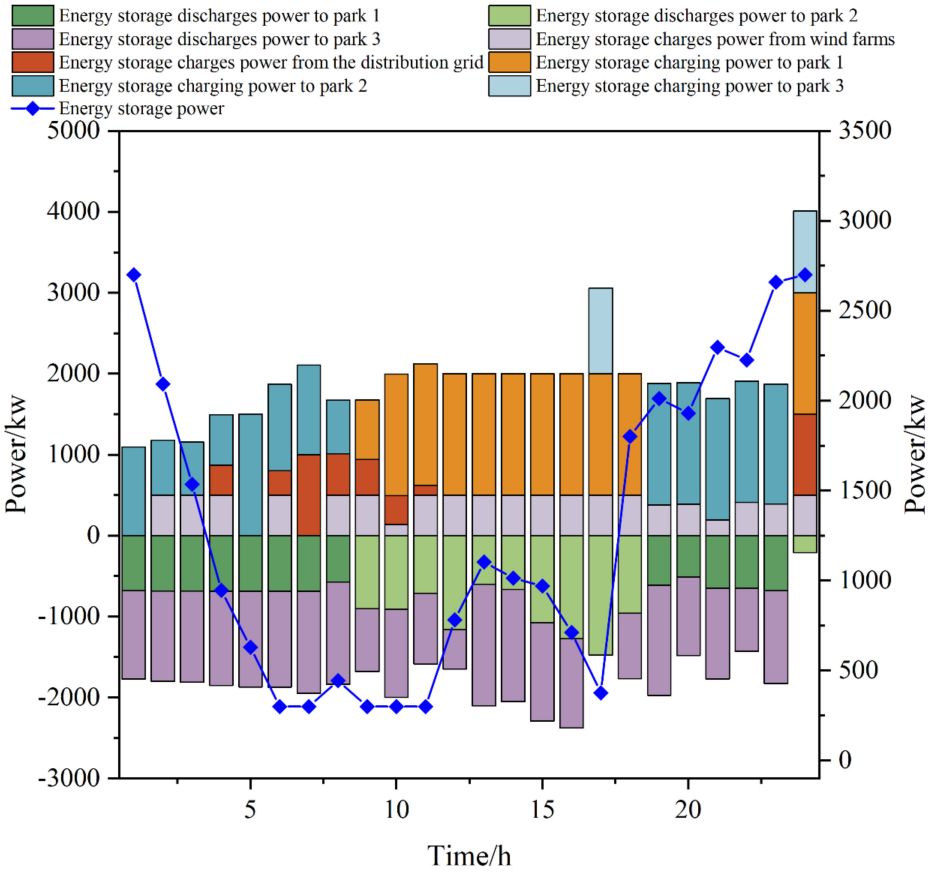

Figure 9. Power balance diagram of energy storage plant.

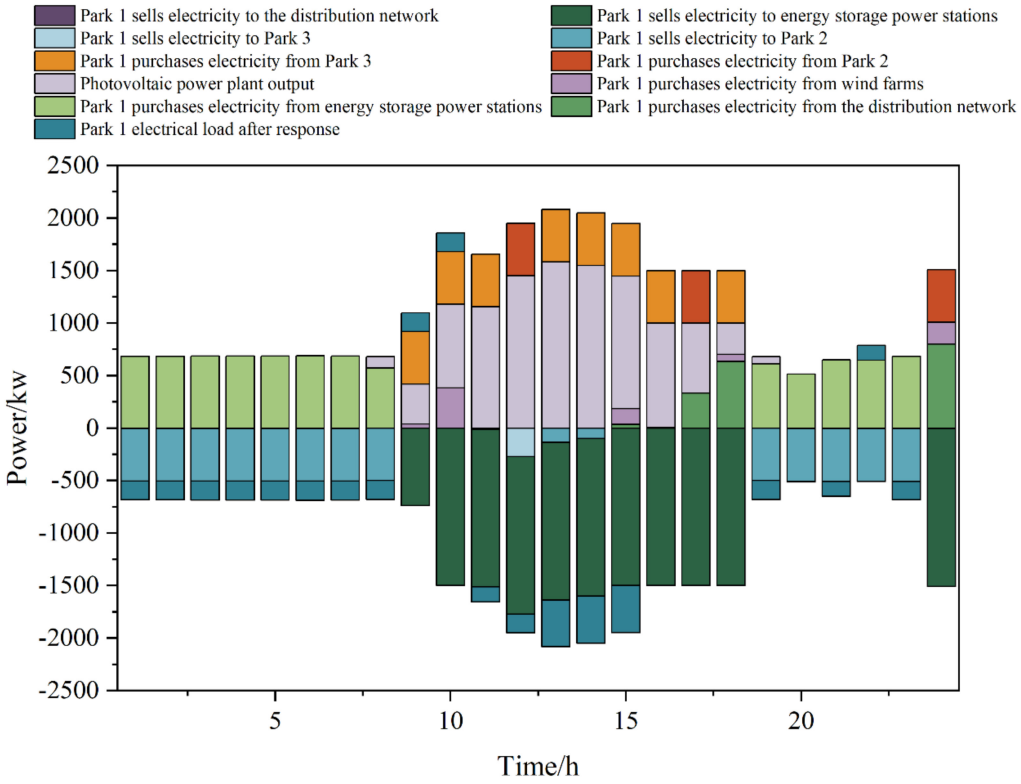

Figure 10. Power balance diagram after optimization of Park 1.

As shown in the figure, the electric load balance of Park 1 primarily consists of inter-park power interactions, power interactions with the storage power station, and new energy outputs from wind and solar sources, coupled with a low level of its own electric load. During the time periods of 00:00–08:00 and 19:00–23:00, Park 1 lacks supply-side output and primarily purchases electricity from the storage power station. Conversely, during the 08:00–18:00 period, when PV output is high and consumption is very low, PV power is mainly sold to the energy storage station.

Figure 11 shows the optimized electric power balance for Park 2. Compared with Park 1, CHP units are added to generate electricity. The flexible operation of CHP can increase the utilization rate of primary energy, so the CHP units operate at full or nearly full load during the dispatch cycle. The remaining loads mainly involve energy interactions with the energy storage plant and other parks. During peak load hours, some power is purchased from the distribution grid to achieve electric power balance in the dispatch cycle. Due to the time-sharing tariff, Park 2 has different power purchase arrangements for different time periods. The energy storage power from 09:00 to 18:00 comes from the centralized storage of PV in Park 1, and the tariff is lower relative to the unit price of park interaction.

The optimization results of the thermal power balance of Park 2 are shown in Figure 12. Since the CHP unit in the model operates in the "setting the heat by electricity" mode, it can be seen from the analysis in Figure 11 that, during the scheduling cycle, the CHP unit operates at or near full load. Therefore, the unit produces heat power close to its maximum capacity, and the remaining heat load is regulated and supplemented by the gas boiler.

Figure 13 shows the optimized power balance of Park 3. As depicted in the figure, Park 3 has a cold load, resulting in increased air conditioning power consumption compared to Park 2. Additionally, Park 3 is already a power-deficient park, and the presence of many users with cold loads and higher air conditioning power consumption exacerbates this shortage. Therefore, besides generating power from its own CHP unit, a significant amount of power needs to be purchased from the storage power plant to ensure power balance. During the 09:00–18:00 period, Park 3 completes multiple electric energy interactions. During the scheduling cycle, Park 3 prioritizes purchasing power from wind farms and

energy storage power stations, and only purchases power from the distribution grid during the two hours of 17:00 and 00:00. CCHP units continue to operate in the "heat by electricity" mode, so the heat load is prioritized to consume the heat produced by CCHP, as in Park 2, with the remaining load supplemented by the gas boiler, as shown in Figure 14.

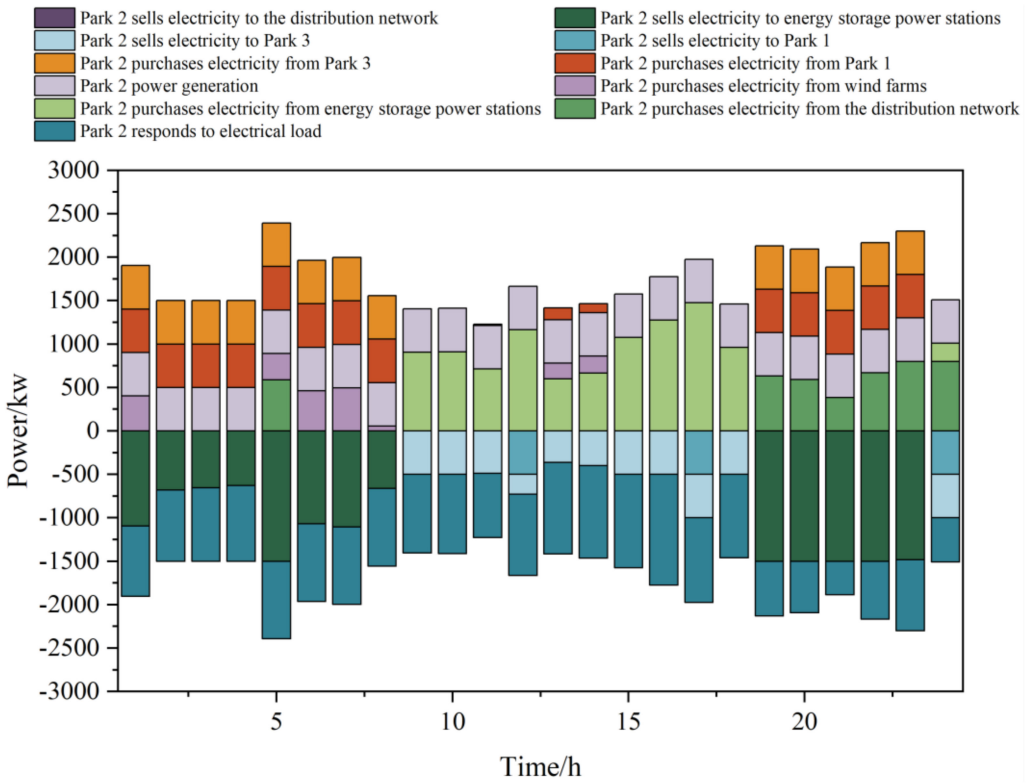

Figure 11. Power balance diagram after optimization of Park 2.

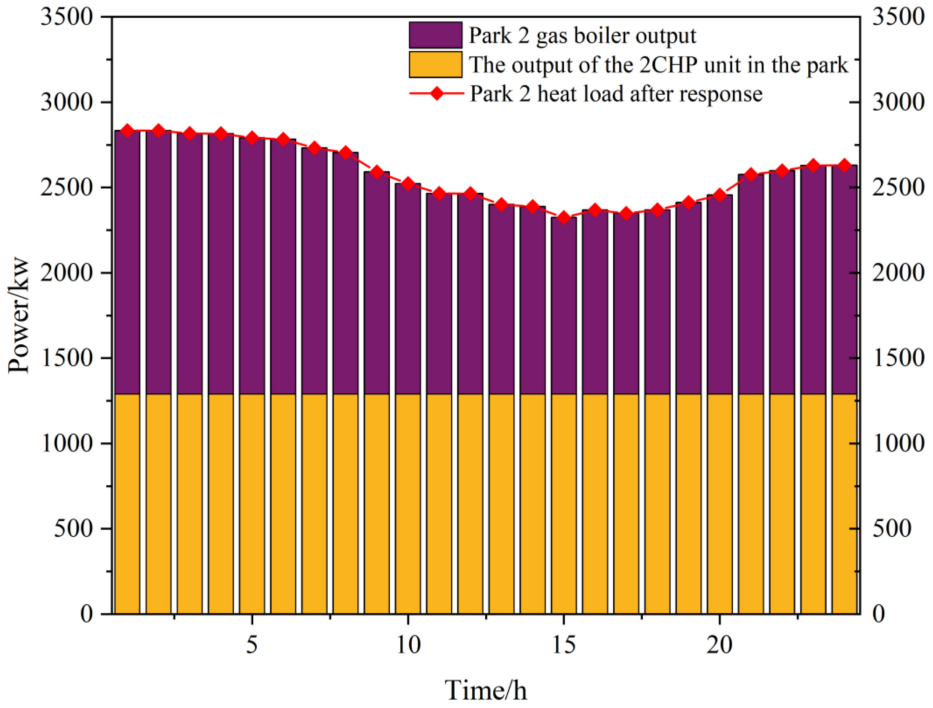

Figure 12. Thermal power balance diagram for Park 2.

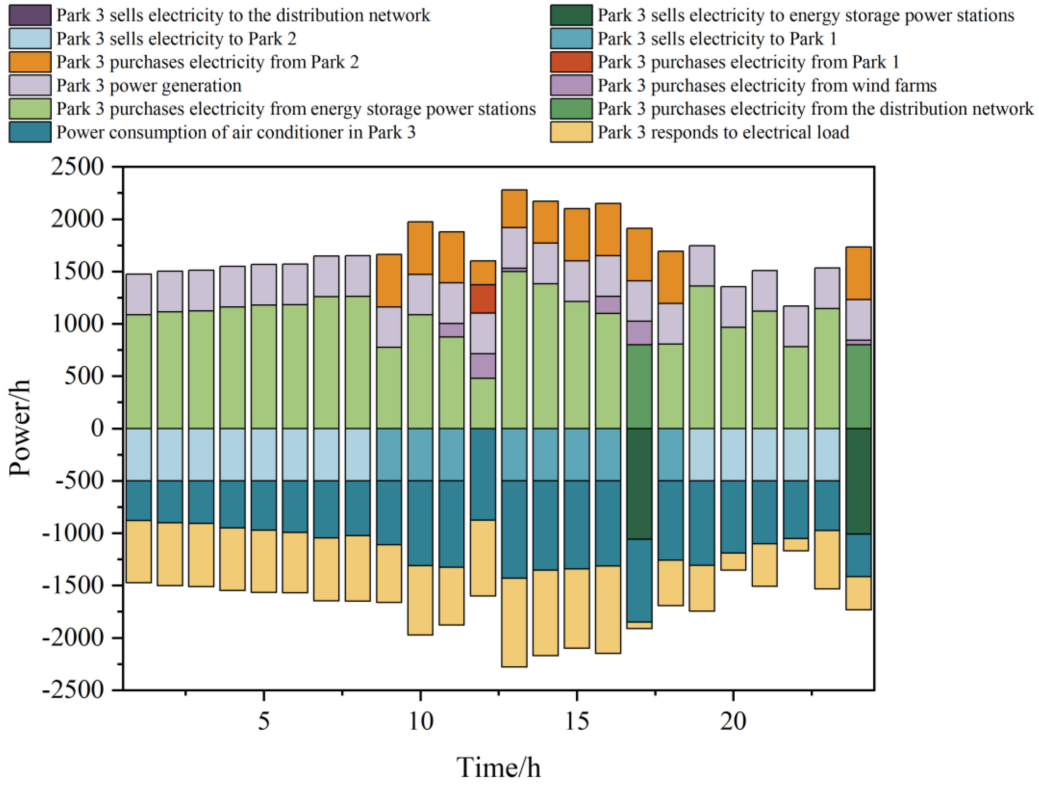

Figure 13. Power balance diagram after optimization of Park 3.

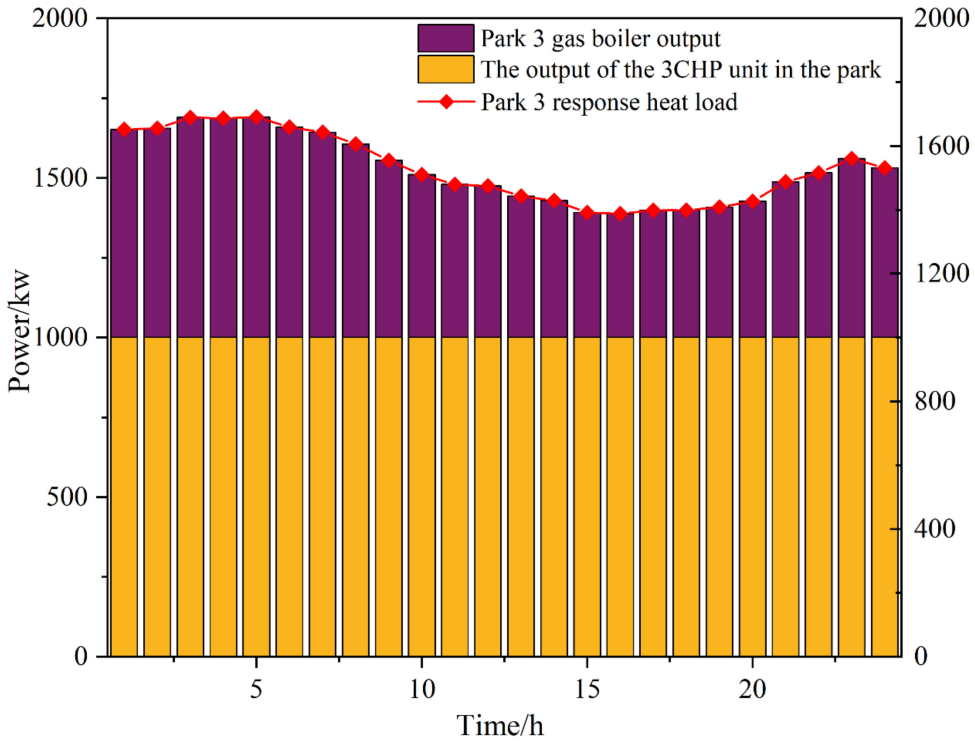

Figure 14. Park 3 thermal power balance diagram.

The results of the optimization of the cooling power balance of Park 3 are shown in Figure 14. From Figure 14, it can be seen that since the CCHP unit uses a lithium bromide refrigerator for cooling, and there are inherent limitations in the absorption and

refrigeration rates, resulting in the output ratio meeting only a small portion of the cooling load demand. As shown in Figure 15, the stationary cooling load is primarily provided by CCHP refrigeration, with the remaining demand met by air-conditioned refrigeration. The controllable cooling load is highly variable throughout the dispatch cycle, characterized by a midday peak and a large percentage of the load, thus requiring air conditioning to manage this load.

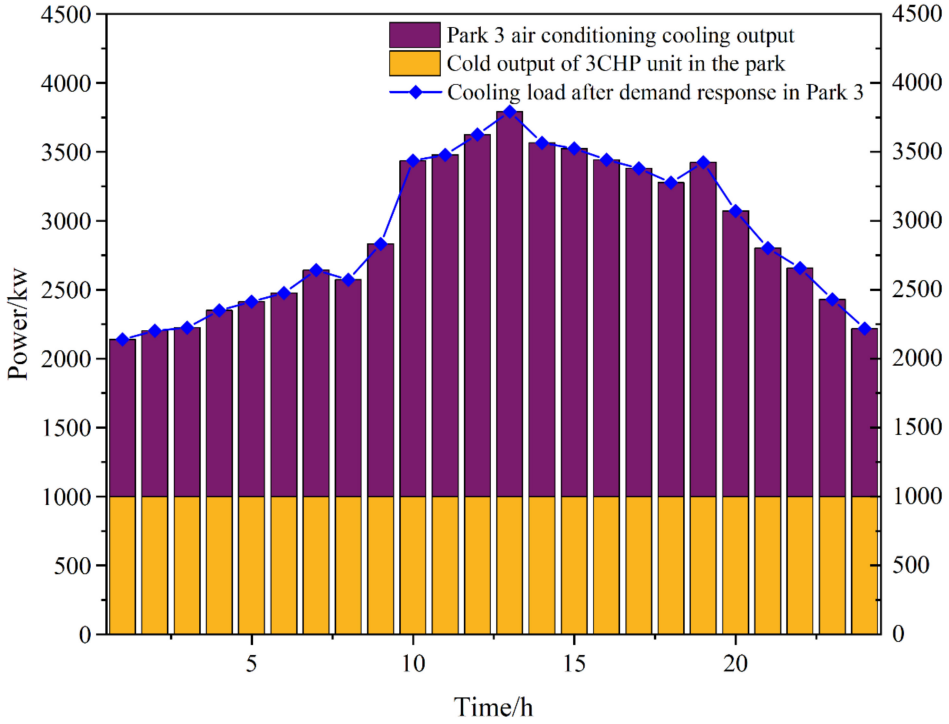

Figure 15. Campus 3 cold power balance diagram.

5. Conclusions

This paper proposes a master–slave game-based optimization scheduling strategy for a multi-energy integrated system (MIES), incorporating integrated demand response and wind-storage coupling. The strategy utilizes a hybrid two-layer optimization framework, combining particle swarm optimization (PSO) with CPLEX, and demonstrates notable advantages in energy trading and internal operation optimization.

First, the proposed method integrates power stations within the MIES to engage in game interactions, solving the Nash equilibrium to find the optimal solution for all parties' interests. This approach significantly enhances the overall system, considering the interests of all participants.

Secondly, by establishing a power interaction channel, multiple stakeholders, the strategy successfully achieves optimal economic performance within the alliance. It efficiently coordinates energy utilization among participants, leading to more effective overall operation.

Additionally, the proposed strategy leverages differentiated multi-loads and multi-type integrated demand response (IDR) for heterogeneous energy flows, effectively shaving peaks and filling valleys for electricity, heat, and cooling loads within reasonable limits. It iteratively optimizes subsidy pricing to enhance user participation and responsiveness.

Overall, the master–slave game-based optimization scheduling strategy proposed in this paper significantly improves the economy and response flexibility of the MIES system through multi-level, multi-agent collaborative optimization, demonstrating its strong potential for future energy system applications.

However, this paper does not address energy transmission losses, and future research will focus on improvements in this area.

Author Contributions: H.S.: methodology, resources, funding acquisition, writing—original draft preparation; H.Z.: validation, formal analysis, writing—original draft preparation; J.J.: data curation, writing—original draft preparation; Q.S.: software, formal analysis, writing—review and editing; Z.D.: investigation, funding acquisition, writing—review and editing. X.T.: formal analysis. All authors have read and agreed to the published version of the manuscript.

Funding: This work was supported in part by the Scientific and Technological Planning Project of Jilin Province (YDZJ202201ZYTS642).

Data Availability Statement: The original contributions presented in the study are included in the article, further inquiries can be directed to the corresponding author.

Conflicts of Interest: The authors declare no conflicts of interest.

Appendix A

Table A1. Energy conversion equipment parameters.

Device Name	English Abbreviation	Conversion Efficiency/COP	Aging Loss Coefficient
Gas boiler	GB	0.9	0.026
Gas turbine	GT	0.35	0.021
Waste heat boiler	WHB	0.68	0.016
Energy storage power station	ESS	0.98	0.013
Air conditioner	AC	3	0.015
Photovoltaic	PV	/	0.039
Wind power	WT	/	0.039
Lithium bromide refrigerator	LBAC	0.72	0.013

Table A2. Time-of-use energy price.

Time	Distribution Network Electricity Sales Price/CNY	Purchase Between Parks Electricity Sales Price/CNY	Wind Farm for Sale Electricity Price/CNY	Energy Storage Power Station Electricity Sales Price/CNY	Natural Gas Price/ CNY/m^3
00:00–8:00	0.35	0.23	0.29	0.29	1.84
8:00–12:00	0.68	0.46	0.57	0.57	2.94
12:00–00:00	1.04	0.71	0.88	0.88	3.84

Appendix B

a_i represents a potential set of possible game strategies; similarly, the speed of the ith particle is the 3T-dimensional vector E, the local optimal strategy of individual particles is the 3T-dimensional vector pbesti, and the global optimal strategy of the particle swarm is the 3T-dimensional vector gbest.

The updated set of particle trading strategies is:

$$\varphi = [a, s] \tag{A1}$$

The equations for particle position and velocity update are:

$$\begin{cases} v_{ij}^{k+1} = \omega \cdot v_{ij}^{k} + c_1 r_1 (pbest_{ij}^{k} - x_{ij}^{k}) + c_2 r_2 (gbest_{ij}^{k} - x_{ij}^{k}) \\ x_{ij}^{k+1} = x_{ij}^{k} + v_{ij}^{k+1} \end{cases} \tag{A2}$$

where ω is the inertia weight; i represents the number of the particle, taking the value of 1, 2, …, n; j represents the j dimension component of the particle, taking the value of 1, 2, …, 3T; k represents the number of iterations; c_1 and c_2 represent the learning factors of the particle, and r_1 and r_2 are the random numbers of [0,1]. The particle speed threshold is set because the particle speed is too large to cause the particle to jump out of the

optimal solution, and the particle speed is too small to cause insufficient search in the optimization space:

$$V_{\min} \le V_{ij}^{k} \le V_{\max} \tag{A3}$$

where $V_{\min}$ and $V_{\max}$ denote the upper and lower limits of particle velocity during the iteration process. The specific values are shown in Table A3 in Appendix B.

For the traditional particle swarm algorithm there are problems such as premature convergence. This paper adopts a linear decreasing strategy for the inertia weights, with larger inertia weights at the early iteration and smaller inertia weights at the end of the iteration. Larger inertia weight is conducive to jumping out of the local optimum, where global search ability is stronger, and smaller inertia weight can be in the vicinity of the global optimum to search accurately, which is conducive to the convergence of the algorithm. The learning factor adopts a nonlinear inverse cosine acceleration strategy. The particles focus on the reference of their own history information when flying in the early iteration, and focus on the reference of the group information when flying in the late iteration to avoid falling into the local convergence. The values of inertia weight ω and learning factors c_1 and c_2 are taken as:

$$\begin{cases} \omega = \omega_{\mathrm{s}} - \frac{k}{k_{\max}} \cdot (\omega_{\mathrm{s}} - \omega_{\mathrm{e}}) \\ c_1 = c_{1e} + (c_{1s} - c_{1e})[1 - \frac{\arccos(-2k/k_{\max}+1)}{\pi}] \\ c_2 = c_{2e} + (c_{2s} - c_{2e})[1 - \frac{\arccos(-2k/k_{\max}+1)}{\pi}] \end{cases} \tag{A4}$$

where $k_{\max}$ is the maximum number of iterations, ω_s and ω_e denote the iterative initial and final values of the inertia weights, and c_s and c_e denote the iterative initial and final values of the learning factors, respectively. The specific values are shown in Table A3.

Table A3. Parameters of the PSO algorithm.

Parameter	Value	Parameter	Value
ω_s	0.9	c_{2e}	0.5
ω_e	0.4	$k_{\max}$	20
c_{1s}	2.5	n	10
c_{1e}	0.5	$\nu_{\min}$	0.5
c_{2s}	2.5	$\nu_{\max}$	−0.5

Appendix C

Existence of the proof of equilibrium solution for the master–slave game:

There are two decision levels with a leader and n followers: P_i (i = 1, 2, ⋯, n), where N = {1, 2, ⋯, n} is the set of composition of the followers; X is the set of strategies of the leader; $\forall i \in N$, which denotes $i = N/i$ and $\forall i \in N$; Y_i is the set of strategies of the first follower $Y = \prod_{i=1}^{n} Y_i$; and $f_i : X \cdot Y \to R$ is the cost function of the i follower. In the parameterized cooperative n-player Nash equilibrium $\Gamma(x) = \{Y, f_i(x, \cdot, \cdot),\ i = \{1, 2, \cdots, n\}$ denotes the set of Nash equilibrium points of the game. $N(x)$ denotes the set of Nash equilibrium points of the game, and the problem is formulated as follows:

$$N(x) = \{y^* = (y_1^*, y_2^*, \cdots, y_n^*) \in Y : f_i(x, y_i^*,) = \inf_{y^i \in X_i} f_i(x, y_i,)\} \tag{A5}$$

The above problem can also be expressed as a set-valued mapping:

$$N: \ X \ \to P_0(\prod_{i=1}^{n} Y_i) \tag{A6}$$

Any strategy $y^* = (y_1^*, y_2^*, \cdots, y_n^*) \in Y$ that satisfies Equation (A5) is said to be an equilibrium of a parametric Nash game $\Gamma(x)$ with y. In a leader–follower game, the leader

and followers occupy the upper and lower levels of decision-making, respectively, forming a typical bilevel optimization problem.

The leader selects a strategy xxx from its strategy set X, and the followers, given x, determine their optimal solutions through Nash equilibrium within their respective strategy sets. This paper seeks to prove the existence of equilibrium solutions for such games under specific assumptions. We assume that the strategy sets X of the leader and Y_i of the followers are non-empty, compact, and convex. Furthermore, the cost function $f_i = (y_1, y_2, \cdots, y_n; x)$ for each follower is continuous with respect to the leader's strategy x and quasiconcave with respect to its own strategy y_i. This ensures that each follower can find its optimal strategy given the fixed strategies of the other followers. The followers' optimal responses are denoted as $y_i^*(x)$, forming a Nash equilibrium at the follower level. We define $N(x)$ as the set mapping of the followers' Nash equilibrium after the leader selects a strategy x. We prove that this mapping is upper semicontinuous, implying that small changes in the leader's strategy result in minimal fluctuations in the followers' Nash equilibrium. By combining the conditions of compactness, convexity, and upper semicontinuity, we apply the Kakutani fixed-point theorem to prove the existence of a fixed point in this mapping, representing the equilibrium solution of the leader–follower game. In summary, under the assumptions of compactness, continuity, quasiconcavity, and upper semicontinuity, this paper proves the existence of a Nash equilibrium in a leader–follower game. This conclusion lays the theoretical foundation for addressing multi-level decision-making problems and can be applied to optimization in complex systems such as energy markets.

Let $G = \{X, Y, f, f_i(x, \cdot, \cdot)\}, i = 1, 2, \cdots, n$ denote the two-stage master–slave game equilibrium problem, which is formulated as $\exists (x^*, y^*) \in X \cdot Y$, such that:

$$f(x^*, y^*) = \sup_{y \in N(x^*)} f(x^*, y) = \inf_{x \in X} \sup_{y \in N(x)} f(x, y), y^* \in N(x^*) \tag{A7}$$

Any strategy group $(x^*, y^*) \in X \cdot Y$ satisfies Equation (A6), and then (x^*, y^*) is said to be an equilibrium point of a master–slave game. The equilibrium conditions of the two-stage master–slave game, as defined by Equation (A7), involve a sequential decision-making process between the leader (master) and the followers (slaves). In this bilevel structure, the leader first selects a strategy x^*, anticipating optimal responses y^* from the followers. The followers then choose strategies that minimize their objective functions, based on the leader's decision. The interaction is governed by a parametric Nash equilibrium, where neither player benefits from unilateral deviations from the equilibrium strategy set (x^*, y^*). The equilibrium is reached under the following assumptions: (1) rationality: Both the leader and the followers are rational players, seeking to optimize their respective objectives, (2) complete information: All players have complete knowledge of the game's structure and the objectives of the other players, and (3) sequential optimality: The leader's decision-making process accounts for the followers' best-response behavior, resulting in a minimax strategy where the leader minimizes the worst-case outcome based on the followers' optimal responses. The condition $\sup_{y \in N(x^*)} f(x^*, y) = \inf_{x \in X} \sup_{y \in N(x)} f(x, y)$ represents the equilibrium, where the leader and followers' strategies satisfy both the supremum and the infimum conditions. This ensures that no player can improve their payoff by deviating from the equilibrium, guaranteeing the stability of the solution in the master–slave game.

Appendix D

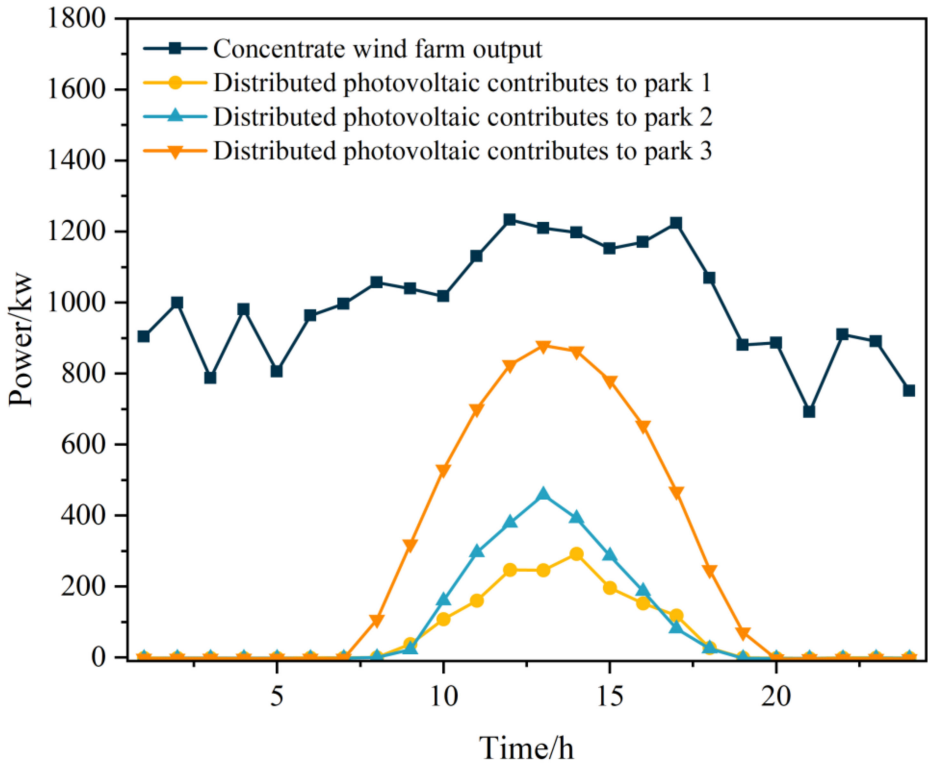

Figure A1. Load forecasting and photovoltaic output forecasting.

References

1. Hannan, M.A.; Ker, P.J.; Mansor, M.; Lipu, M.S.H.; Al-Shetwi, A.Q.; Alghamdi, S.M.; Begum, R.A.; Tiong, S.K. Recent advancement of energy internet for emerging energy management technologies: Key features, potential applications, methods and open issues. *Energy Rep.* **2023**, *10*, 3970–3992. [CrossRef]
2. Li, P.; Wang, Z.; Liu, H.; Wang, J.; Guo, T.; Yin, Y. Bi-level optimal configuration strategy of community integrated energy system with coordinated planning and operation. *Energy* **2021**, *236*, 121539. [CrossRef]
3. Li, P.; Wang, Z.; Wang, N.; Yang, W.; Li, M.; Zhou, X.; Yin, Y.; Wang, J.; Guo, T. Stochastic robust optimal operation of community integrated energy system based on integrated demand response. *Int. J. Electr. Power Energy Syst.* **2021**, *128*, 106735. [CrossRef]
4. Guo, Z.; Zhang, R.; Wang, L.; Zeng, S.; Li, Y. Optimal operation of regional integrated energy system considering demand response. *Appl. Therm. Eng.* **2021**, *191*, 116860. [CrossRef]
5. Sudhoff, R.; Derzbach, R.; Schreck, S.; Thiem, S.; Niessen, S. On the operation and implications of grid-interactive renewable energy communities. *Sustain. Energy Grids Netw.* **2024**, *38*, 101390. [CrossRef]
6. Zhang, Z.; Jiang, P.; Liu, Z.; Fu, L.; Wang, P. Capacity optimal configuration and collaborative planning of multi-region integrated energy system. *Energy* **2023**, *278*, 127970. [CrossRef]
7. Zhang, W.; Xu, Y. Distributed optimal control for multiple microgrids in a distribution network. *IEEE Trans. Smart Grid* **2018**, *10*, 3765–3779. [CrossRef]
8. Zhao, Q.; Su, C.-W.; Qin, M.; Umar, M. Is global renewable energy development a curse or blessing for economic growth? Evidence from China. *Energy* **2023**, *285*, 129403. [CrossRef]
9. Fang, Y.; Zhao, S.; Chen, Z. Multi-objective unit commitment of jointly concentrating solar power plant and wind farm for providing peak-shaving considering operational risk. *Int. J. Electr. Power Energy Syst.* **2021**, *137*, 107754. [CrossRef]
10. Cao, J.; Qin, Z.; Gao, X.; Pu, T.; Zhu, W.; Ke, S.; Shen, X. Study of aerodynamic performance and wake effects for offshore wind farm cluster. *Ocean Eng.* **2023**, *280*, 114639. [CrossRef]
11. Zhang, Z.; Ding, T.; Zhou, Q.; Sun, Y.; Qu, M.; Zeng, Z.; Ju, Y.; Li, L.; Wang, K.; Chi, F. A review of technologies and applications on versatile energy storage systems. *Renew. Sustain. Energy Rev.* **2021**, *148*, 111263. [CrossRef]
12. Tan, K.M.; Babu, T.S.; Ramachandaramurthy, V.K.; Kasinathan, P.; Solanki, S.G.; Raveendran, S.K. Empowering smart grid: A comprehensive review of energy storage technology and application with renewable energy integration. *J. Energy Storage* **2021**, *39*, 102591. [CrossRef]

13. Argyrou, M.C.; Christodoulides, P.; Kalogirou, S.A. Energy storage for electricity generation and related processes: Technologies appraisal and grid scale applications. *Renew. Sustain. Energy Rev.* **2018**, *94*, 804–821. [CrossRef]
14. Gao, J.; Gao, F.; Yang, Y.; Wu, H.; Zhang, Y.; Liang, P. Configuration optimization and benefit allocation model of multi-park integrated energy systems considering electric vehicle charging station to assist services of shared energy storage power station. *J. Clean. Prod.* **2022**, *336*, 130381. [CrossRef]
15. Zhang, Y.; Wei, A.; Zou, S.; Luo, D.; Zhu, H.; Zhang, N. A planning scheme for energy storage power station based on multi-spatial scale model. *Energy Rep.* **2023**, *9*, 591–600. [CrossRef]
16. Miletić, M.; Pandžić, H.; Yang, D. Operating and investment models for energy storage systems. *Energies* **2020**, *13*, 4600. [CrossRef]
17. Zhou, Y.; Ma, Z.; Shi, X.; Zou, S. Multi-agent optimal scheduling for integrated energy system considering the global carbon emission constraint. *Energy* **2024**, *288*, 129732. [CrossRef]
18. Li, K.; Ye, N.; Li, S.; Wang, H.; Zhang, C. Distributed collaborative operation strategies in multi-agent integrated energy system considering integrated demand response based on game theory. *Energy* **2023**, *273*, 127137. [CrossRef]
19. Liu, J.; Wang, A.; Qu, Y.; Wang, W. Coordinated operation of multi-integrated energy system based on linear weighted sum and grasshopper optimization algorithm. *IEEE Access* **2018**, *6*, 42186–42195. [CrossRef]
20. Liao, W.; Xiao, F.; Li, Y.; Peng, J. Comparative study on electricity transactions between multi-microgrid: A hybrid game theory-based peer-to-peer trading in heterogeneous building communities considering electric vehicles. *Appl. Energy* **2024**, *367*, 123459. [CrossRef]
21. Wang, S.; Chen, H.; Gong, C.; Shang, Y.; Wang, Z. The Operation Strategy of a Multi-Microgrid Considering the Interaction of Different Subjects' Interests. *Energies* **2024**, *17*, 4883. [CrossRef]
22. Chen, W.; Wang, J.; Yu, G.; Chen, J.; Hu, Y. Research on day-ahead transactions between multi-microgrid based on cooperative game model. *Appl. Energy* **2022**, *316*, 119106. [CrossRef]
23. Baghbanzadeh, D.; Salehi, J.; Gazijahani, F.S.; Shafie-Khah, M.; Catalão, J.P. Resilience improvement of multi-microgrid distribution networks using distributed generation. *Sustain. Energy Grids Netw.* **2021**, *27*, 100503. [CrossRef]
24. Zhao, B.; Wang, X.; Lin, D.; Calvin, M.M.; Morgan, J.C.; Qin, R.; Wang, C. Energy management of multiple microgrids based on a system of systems architecture. *IEEE Trans. Power Syst.* **2018**, *33*, 6410–6421. [CrossRef]
25. Resende, F.O.; Gil, N.J.; Lopes, J.A.P. Service restoration on distribution systems using multi-microgrids. *Eur. Trans. Electr. Power* **2011**, *21*, 1327–1342. [CrossRef]
26. Zhou, Y.; Wu, H.; Li, Y.; Xin, H.; Song, Y. Dynamic dispatch of multi-microgrid for neighboring islands based on MCS-PSO algorithm. *Autom. Electr. Power Syst.* **2014**, *38*, 204–210.
27. Du, J.N.; Han, X.Q.; Li, T.J.; Wang, J. Optimization strategy of multi microgrid electric energy cooperative operation considering electricity price uncertainty and game cheating behaviors. *Power Syst. Technol.* **2022**, *46*, 4217–4230.
28. Tang, S.; He, S.; Hu, B.; Fan, X. Shared energy storage-multi-microgrid operation strategy based on multi-stage robust optimization. *J. Energy Storage* **2024**, *97*, 112785. [CrossRef]
29. Lu, Q.; Guo, Q.; Zeng, W. Optimal dispatch of community integrated energy system based on Stackelberg game and integrated demand response under carbon trading mechanism. *Appl. Therm. Eng.* **2022**, *219*, 119508. [CrossRef]
30. Li, Y.; Li, K.; Yang, Z.; Yu, Y.; Xu, R.; Yang, M. Stochastic optimal scheduling of demand response-enabled microgrids with renewable generations: An analytical-heuristic approach. *J. Clean. Prod.* **2022**, *330*, 129840. [CrossRef]
31. Li, Y.; Han, M.; Shahidehpour, M.; Li, J.; Long, C. Data-driven distributionally robust scheduling of community integrated energy systems with uncertain renewable generations considering integrated demand response. *Appl. Energy* **2023**, *335*, 120749. [CrossRef]
32. Pandey, V.C.; Gupta, N.; Niazi, K.; Swarnkar, A.; Thokar, R.A. Modeling and assessment of incentive based demand response using price elasticity model in distribution systems. *Electr. Power Syst. Res.* **2022**, *206*, 107836. [CrossRef]
33. Li, P.; Wang, Z.; Yang, W.; Liu, H.; Yin, Y.; Wang, J.; Guo, T. Hierarchically partitioned coordinated operation of distributed integrated energy system based on a master-slave game. *Energy* **2020**, *214*, 119006. [CrossRef]
34. Zhu, B.; Wang, D. Master–Slave Game Optimal Scheduling for Multi-Agent Integrated Energy System Based on Uncertainty and Demand Response. *Sustainability* **2024**, *16*, 3182. [CrossRef]
35. Huang, W.; Zhang, B.; Ge, L.; He, J.; Liao, W.; Ma, P. Day-ahead optimal scheduling strategy for electrolytic water to hydrogen production in zero-carbon parks type microgrid for optimal utilization of electrolyzer. *J. Energy Storage* **2023**, *68*, 107653. [CrossRef]
36. Deng, H.; Wang, J.; Shao, Y.; Zhou, Y.; Cao, Y.; Zhang, X.; Li, W. Optimization of configurations and scheduling of shared hybrid electric-hydrogen energy storages supporting to multi-microgrid system. *J. Energy Storage* **2023**, *74*, 109420. [CrossRef]
37. Zhang, J.; Liu, Z. Low carbon economic scheduling model for a park integrated energy system considering integrated demand response, ladder-type carbon trading and fine utilization of hydrogen. *Energy* **2024**, *290*, 130311. [CrossRef]
38. Yang, X.; Chen, Z.; Huang, X.; Li, R.; Xu, S.; Yang, C. Robust capacity optimization methods for integrated energy systems considering demand response and thermal comfort. *Energy* **2021**, *221*, 119727. [CrossRef]
39. Ma, Y.; Zhang, M.; Yang, H.; Wang, X.; Xu, J.; Hu, X. Decentralized and coordinated scheduling model of interconnected multi-microgrid based on virtual energy storage. *Int. J. Electr. Power Energy Syst.* **2023**, *148*, 108990. [CrossRef]

40. Zhou, B.; Zhang, Y.; Zang, T.; Hua, W. Optimal dispatching of distribution network considering system flexibility and user thermal comfort. *IEEE Access* **2021**, *9*, 107895–107908. [CrossRef]
41. Eid, A.; Mohammed, O.; El-Kishky, H. Efficient operation of battery energy storage systems, electric-vehicle charging stations and renewable energy sources linked to distribution systems. *J. Energy Storage* **2022**, *55*, 105644. [CrossRef]